Sensitivities to a Light Scalar Particle Using Muon Decay, Kaon Decay, and Electron-Positron Annihilation

by

Nicholas Lange
B.Sc., University of Victoria, 2012

A Thesis Submitted in Partial Fulfillment of the
Requirements for the Degree of

MASTER OF SCIENCE

in the Department of Physics and Astronomy

Sensitivities to a Light Scalar Particle Using Muon Decay, Kaon Decay, and Electron-Positron Annihilation

by

Nicholas Lange
B.Sc., University of Victoria, 2012

Supervisory Committee

Dr. Maxim Pospelov, Supervisor
(Department of Physics and Astronomy)

Dr. Adam Ritz, Departmental Member
(Department of Physics and Astronomy)

Dr. Michel Lefebvre, Departmental Member
(Department of Physics and Astronomy)

Supervisory Committee

Dr. Maxim Pospelov, Supervisor
(Department of Physics and Astronomy)

Dr. Adam Ritz, Departmental Member
(Department of Physics and Astronomy)

Dr. Michel Lefebvre, Departmental Member
(Department of Physics and Astronomy)

ABSTRACT

There are several anomalies within the Standard Model of particle physics that may be explained by means of light new physics. These may be associated with muons, with the gyromagnetic ratio of the muon being different from theory at the level of 3.4σ, and with the 7σ muonic Hydrogen proton radius extraction. Previous, current, and new experiments may be able to place stringent limits on the existence of a new scalar force, with a coupling to leptons proportional to their mass. We investigate the sensitivity to the parameter space of the muon decay experiment Mu3e, the kaon decay experiments NA48/2 and NA62, and the experiments at asymmetric electron-positron colliders, BaBar, Belle, Belle2. Using Monte Carlo techniques to generate events for processes corresponding to each experiment, we find that these experiments could be sensitive to muonic couplings down to 10^{-5}, and over a wide mass range of 10 MeV $-$ 3.5 GeV, fully covering the parameter space relevant for explanations of these anomalies. The possibility exists to later extend to masses up to 10 GeV.

Contents

List of Tables

List of Figures

ACKNOWLEDGEMENTS

I would like to thank:

my parents, Henry Lange and Elisabeth Jahren, for giving me an environment where I can grow up to enjoy learning, and their never ending love and support.

Kayla McLean and the other graduate students, for keeping me human throughout this journey.

Dr. Maxim Pospelov, for taking me under his wing, providing an interesting project to work on, and for knowing when to guide me and when to let me explore.

University of Victoria and the Department of Physics and Astronomy, for giving me both the point of view of an undergraduate student and a graduate student, for providing funding and scholarships, and for an office to call my own.

Perimeter Institute for Theoretical Physics, for providing a place to learn, be productive, and meet new people.

I can live with doubt, and uncertainty, and not knowing. I think it's much more interesting to live not knowing than to have answers which might be wrong. I have approximate answers, and possible beliefs, and different degrees of certainty about different things, but I'm not absolutely sure of anything. There are many things I don't know anything about, such as whether it means anything to ask "Why are we here?" I might think about it a little bit, and if I can't figure it out then I go on to something else. But I don't have to know an answer. I don't feel frightened by not knowing things, by being lost in the mysterious universe without having any purpose — which is the way it really is, as far as I can tell. Possibly. It doesn't frighten me.

Richard Feynman

DEDICATION

To mom, dad, and Kayla for all their love and encouragement.

Chapter 1

Introduction

The Standard Model (SM) of particle physics stands as one of our most scrutinized and well-tested theories in physics. Very few discrepancies have been found between the model and reality, within the realm of experimental particle physics. The discovery of the Higgs boson in July 2012 stands as the most recent example, with the measured quantities thus far matching the Standard Model Higgs boson. However, it must be the case that the theory is incomplete, as we currently do not know how to incorporate the effects of quantum gravity into the model. In order to make progress, one can look to the few experiments that provide some level of discrepancy; these could act as a loose string that we can use to unravel the current mysteries of particle physics.

Historically, experimental anomalies have been used as a foundation to construct our understanding of particle physics. For example, the solar neutrino problem was an anomaly that led to the eventual discovery of neutrino oscillations; the Homestake experiment [1] in the 1960s would house a large vat of perchloroethylene underground, looking for evidence of neutrino capture via $\nu_e + {}^{37}\mathrm{Cl} \rightarrow {}^{37}\mathrm{Ar} + e^-$. The results compared to theoretical calculations yielded a deficit by a factor of three. Other experimental efforts were also established to measure the flux of solar neutrinos, such as SAGE [2], GALLEX [3], SNO [4], Kamiokande and Super-Kamiokande [5, 6]. Eventually, the realization was that the Homestake experiment was only sensitive to one of the three neutrino flavours, while SNO was the first experiment able to detect the oscillations put forth in 1968 that would lead on to explain the missing solar neutrinos [7].

Muons have long been a source of mystery within the physics community. They were discovered in 1936 by Carl Anderson and Seth Neddermyer, who observed the distinct curvature of the muon in a magnetic field, compared to that of electrons and

protons. Since then, there have been many questions regarding the properties of this particle. One of the deeper questions of the Standard Model concerns the number of generations of leptons: Why is it that we observe three generations, the electron, muon, and tau? Within the Standard Model, each generation of lepton differs only by the mass assigned to them.

However, while this can be viewed as an aesthetic problem with the model, at least two experimental efforts have revealed discrepancies between the Standard Model muons and reality. In particular, the muon's spin magnetic moment g appears to be different at the level of 10^{-8} which, although a small number, represents a 3.4σ discrepancy between experiment and theory [8]. It is important to note that many tests have been performed with muons that are consistent with the SM. The TWIST experiment at TRIUMF has provided high precision measurements (a few parts in $10,000$) of distributions of decay products with polarized muons [9]. Universality of the electron and muon has also been tested in pion [10], kaon [11], and Z-boson decays [12].

Additionally, one can perform experiments on *muonic Hydrogen* (μH) in which the electron orbiting the proton is replaced with a muon. For both cases of electronic Hydrogen (H) and μH, the proton charge radius r_p, which will be better defined later in the thesis, can be extracted. Peculiarly, the two results differ by a significant amount, $\Delta(r_p^2) = (r_p^2)_{\text{electrons}} - (r_p^2)_{\text{muons}} = 0.06$ fm^2, and stand at a 7σ discrepancy from zero [13]. Regardless of whether H or μH is used, the extraction of the proton charge radius should remain unchanged. This leads to an exciting avenue to search for new physics, and may give some hints to a new physics role for the muon in such a system.

If new physics has the potential to solve some of these problems, then we must know where to look for the new physics. We will take $\hbar = c = 1$ in this thesis. Since we have that $G_F \ll \Delta(r_p^2)$, this provides a good indication that, to explain the proton radius discrepancy, we should look for a carrier of a new gauge or Yukawa force much lighter than the electroweak scale. A light new mediator may be able to solve these issues, such as the dark photon. It is the goal of this thesis to study the sensitivity limits of detection of such a new light mediator. In our case we consider a scalar, ϕ, which violates lepton universality by coupling to leptons proportionally to their mass, very similarly to the SM Higgs boson. This can have implications for a whole range of experiments, especially at the intensity frontier where precision physics measurements are possible. A schematic of the landscape is shown in Fig. 1.1.

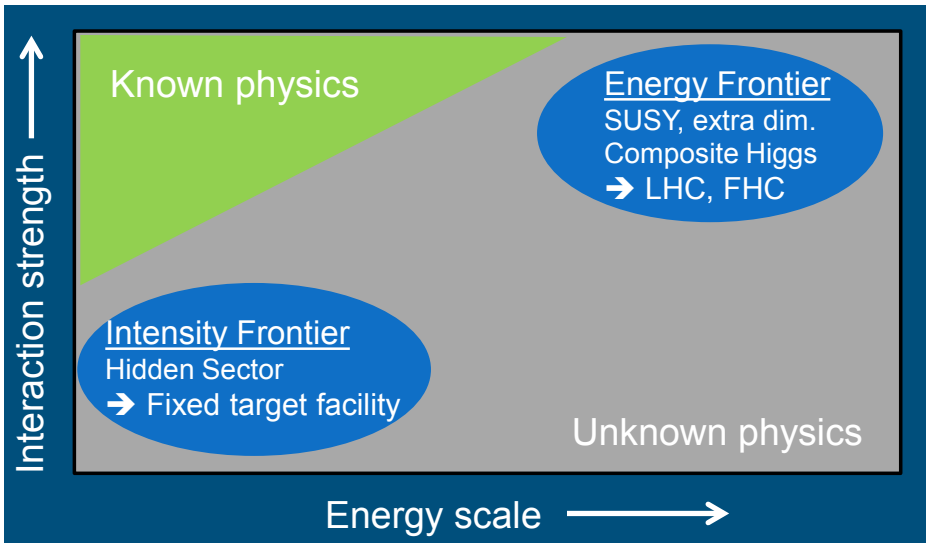

Figure 1.1: Schematic of the frontiers available to experimental particle physics from [14]. The SM lives in the upper left corner. In order to access heavy physics, such as the top or the Higgs, one must turn to the energy frontier with high energy colliders such as the LHC. Lightly coupled new physics is easier to access where there are many collisions or decays in a short period of time, provided that the energies required to produce the new physics are not large.

The experiment Mu3e will have $\mathcal{O}(10^{16})$ total muon decays, so we must investigate how the new force carrying particle interacts with the muon decay signature studied there. Similarly, the experiments NA48/2 and NA62 study $\mathcal{O}(10^{11})$ kaon decays, and we can use this to place sensitivity limits on the strength of the coupling of the new particle. Finally, asymmetric e^+e^- colliders with their associated detectors, like BaBar, Belle, and Belle2, can examine higher energy ranges up to 10.58 GeV, where the tau lepton becomes kinematically accessible and would strongly couple to our new particle. Combining these regimes yields sensitivity over a wide range of masses, from 10 MeV all the way up to 3.5 GeV. The signal processes we will be investigating are the following:

1. $\mu^+ \to e^+\nu_e\bar{\nu}_\mu\phi,\ \phi \to e^+e^-$
2. $K^+ \to \mu^+\nu_\mu\phi,\ \phi \to \ell^+\ell^-$
3. $e^+e^- \to \tau^+\tau^-\phi,\ \phi \to \ell^+\ell^-$

The signature we will be looking for is a spectrally peaked feature where the invariant pair mass can reconstruct the mass of the scalar, $m_{\ell\ell} = m_\phi$.

This thesis contains six core components. The first of these is this short introduction to the problem and motivation. Here we provide a small summary of the contents of each chapter.

Chapter 2 discusses the physical motivations for this project briefly. The main focus is on the apparent anomalies that lie within the Standard Model with emphasis on the muon and lepton flavour violation. Here we will discuss the proton radius problem and the $(g-2)_\mu$ discrepancy. This chapter will stand as the summary of the experimental hints that motivate us to pursue this project. From this, we will see that a candidate for solving these problems is a new scalar force, that so far has received less attention in the literature compared to that of a vector mediator. Later, we will include the restrictions from $(g-2)_\mu$ in our final results of the scalar. This candidate particle will then be the focus for the rest of the thesis, and the limits on the sensitivity of detection will be the final result.

Chapter 3 will examine each experiment in enough detail to place sensible limits on the scalar particle, or derive sensitivity to it for future experiments. These experiments will span the mass range of a few MeV up to 10 GeV. To do this, three classes of experiments will be examined: muon decay, kaon decay, and e^+e^- collisions. Muon decay will be studied in the context of the upcoming Mu3e experiment, which provides a large number of muon decays to work with. Kaon decay at the finished experiment NA48/2, and the upcoming NA62 experiment, will provide access to mediator masses above the muon mass. Finally, e^+e^- collisions at a centre of mass energy of 10.58 GeV, as analyzed by the B-factories BaBar, Belle, and Belle2, will provide the greatest coverage of masses, as well as access to the heaviest leptons.

Chapter 4 provides the prescription of tools that we use and the analytical methods in which we extract our limits. The tools include the Monte Carlo generator MadGraph and other utility tools to interface with the generator. These are used to generate large numbers of signal and background events, in order to study the sensitivity to our model, as finding an analytic expression for some of these decay rates and cross sections can be difficult. Our sensitivity extraction procedure is also covered here, where we precisely define what we claim an experiment's upper-limit sensitivity is.

Chapter 5 contains the results of this work, which are the existing and potential constraints on scalar coupling strength, in the experiments listed above. Each process analyzed is documented here in detail and the resulting sensitivity is given. This includes an explicit detailing of the backgrounds that can affect our overall sensitivity,

as well as how we bin our data, generated or otherwise.

Chapter 6 will conclude the thesis, with a summary of the work completed and results. There will also be some brief comments on future, related work.

Chapter 2

Brief Review of Interesting Muonic Features

The main motivation for the thesis is that there exist experimental anomalies that have yet to be explained, or else they will inevitably be found to be statistically insignificant. This chapter is dedicated to investigating these anomalies in detail. There are two main experimental results that motivate light new physics for our purposes:

1. The proton radius puzzle, in which the proton radius is extracted from μH.
2. $(g-2)$ for the muon, which may be explained by loops of light mediators.

We will also discuss an alternative theory to the scalar, a vector known as the dark photon, that we put forward to test and which may also solve the problems above. Both of these concern the muon, which may provide a hint for where to look for new interesting phenomenon not yet explained by the SM. Within the SM there is no lepton flavour violation, except when one adds neutrino masses; at this point charged lepton flavour violation becomes allowed, but it is suppressed by the incredibly small difference of the neutrino's mass squared, normalized to the weak scale coupling G_F. Another SM particle that breaks lepton universality between the electron and muon is the SM Higgs. The exchange of a Higgs boson at low energy gives rise to the four fermion interaction term

$$\frac{1}{m_h^2}\frac{m_i m_j}{v^2}\bar{\ell}_i\ell_i\bar{\ell}_j\ell_j \tag{2.1}$$

with m_h being the Higgs mass, and v as the Higgs vacuum expectation value (vev). This interaction is suppressed due to the small masses of the leptons, the large mass of the Higgs, and the even larger vev. Any possible effect from equation 2.1 is tiny, making it irrelevant for the phenomenological signatures we discuss. This tells us that, if we take into account the masses of the charged leptons correctly, then physics should be no different when we replace an electron with a muon. Of course this has limits, since the muon can decay to an electron and anti-muon neutrino, and the electron has no decay modes that we are aware of, but this is more a question of allowable kinematics. To have fundamentally different interactions between a muon and other SM particles would be a smoking gun for new physics.

2.1 Proton Radius Puzzle

As has been mentioned a few times already in this thesis, if one does experiments to extract the proton radius using μH, a drastically different result is obtained compared to simple H. In this section we will summarize how this is extracted and potential solutions, including the scalar we put forward, following mostly [13].

First, there are multiple methods which are currently used to extract the proton radius from electronic Hydrogen, H. These methods typically have large error bars, but are consistent with each other, and yield a combined uncertainty of $\sim 0.6\%$. The experiments to extract the proton radius from H are either done using electron-proton scattering, or by measuring energy levels of the Hydrogen system.

For non-relativistic scattering experiments, the differential cross section is given by

$$\frac{d\sigma}{d\Omega} = \left(\frac{\alpha}{4E\sin^2(\theta/2)}\right)^2 \times \left(G(Q^2)\right)^2 \tag{2.2}$$

with the first term being the typical scattering of an electron off of a point-like proton, and the second term correcting for the finite size of the proton. The second term is called a *form factor* and depends on the momentum transfer between the electron and proton. Moving to a relativistic system, as is required for any electron-proton scattering experiment, we find a similar expression

$$\frac{d\sigma}{d\Omega} = \frac{4\alpha^2\cos^2(\theta/2)}{Q^4}\frac{E'^3}{E} \times \frac{1}{1+\tau}\left(G_E^2(Q^2) + \frac{\tau}{\epsilon}G_M^2(Q^2)\right) \tag{2.3}$$

with $\tau = Q^2/4M^2$, $1/\epsilon = 1 + 2(1+\tau)\tan^2(\theta/2)$, and with E' and E being the outgoing and incoming energies of the electron in the lab frame. The first term is now the cross section when scattering an unpolarized spin-1/2 electron off of a pointlike spin-0 target. Also the form factors are now separated into the electric and magnetic components.

To define the proton radius, we look to the non-relativistic system and find that $G(Q^2) = 1 - \frac{1}{6}\langle r^2\rangle Q^2 + \cdots$, which has dependence on the average squared radius. Promoting this to a definition, we define the charge radius to be

$$R_E^2 \equiv -6\frac{dG_E}{dQ^2}|_{Q^2=0} \tag{2.4}$$

Experiments looking to extract the proton charge radius using *e-p* scattering must measure this form factor. For the proton, the average squared charged radius is often written as r_p^2.

One can also measure the Lamb shift, which is the difference between the $2S_{1/2}$ and $2P_{1/2}$ levels. Additionally, for the Hydrogen based extraction, the optical transitions are also used. The correction to the splittings is given by

$$\Delta E = a\mathrm{Ry} + bR_E^2 \tag{2.5}$$

for known coefficients a and b. If one measures two splittings at a time, both the Rydberg constant and the proton charge radius can be extracted simultaneously, and this is precisely what is done. The overall result is $R_E = 0.8775(51)$ fm when the spectroscopic and scattering results are all combined, from CODATA [15].

Similarly, a group performed the same extraction by measuring the Lamb shift of μH [16, 17] and found $R_E = 0.84087(39)$ fm after measuring two hyperfine components of the $2S - 2P$ transition in muonic Hydrogen. This is the 7σ discrepancy between the muonic Hydrogen and electric Hydrogen. This work was carried out by the Charge Radius Experiment with Muonic Hydrogen (CREMA) collaboration at the Paul Scherrer Institute (PSI). A beam of muons are slowed and sent into a target of hydrogen, where they are captured in many high energy states. They then proceed to cascade down to the $1S$ or $2S$ state. A laser is then shined onto the μH to bump the long-lived $2S$ states up to the $2P$ states, which readily decay to the $1S$ state and give off a characteristic X-ray. The frequency that the laser is tuned at will then give the splitting and the proton radius can be read off, provided one has an X-ray detector that can signal when you have tuned the laser correctly. The exact details

of determining the splitting are not important to our discussion, so this description shall suffice.

The conclusion is that one of three possibilities should account for this discrepancy:

- There are unknown/unexpected QCD corrections that can provide the necessary correction.
- The extraction of R_E from the collection of electronic measurements is problematic and prone to error
- There is new physics that violates lepton universality.

First, the unknown QCD corrections from hadronic behaviour are investigated in [13]. The two-photon interaction between a muon and proton involves two unknown functions and a Wick rotation to extract the amplitudes. However, during the Wick rotation, one of the integrals used may not converge, leaving a piece leftover that must be subtracted off that is unknown. Limits are placed on this "subtraction function" for low Q^2, which are not large enough to explain the proton radius; however, it is possible to construct the subtraction function in such a way that one can have a large contribution to the proton radius [18], although usually with the caveat of a large difference in masses between the proton and neutron being introduced.

Alternative determinations of r_p^2 are also being investigated at proposed experiments like the MUon Scattering Experiment (MUSE) at PSI [19], and the Proton Radius experiment (PRAD) at Jefferson Lab [20]. MUSE will extract the proton charge radius with μ-p scattering, which will complement the e-p scattering and complete measurements using muons and electrons for both scattering and spectroscopy. PRAD plans to perform e-p scattering, but with a large acceptance calorimeter as opposed to a traditional magnetic spectrometer method. In this experiment, the systematics that dominated previous e-p scattering results are not present, and instead detector efficiencies and angular acceptances are introduced. This will give access to the derivative of the form factor for Q^2 in the range $\mathcal{O}(10^{-4} - 10^{-2})$ GeV^2.

In this thesis, we focus on the possibility of new physics, however remote this possibility may seem. It is useful to note that some models could potentially solve both the proton radius problem and the discrepancy of $(g-2)_\mu$. We may use this as a motivation during model building.

2.2 $(g-2)_\mu$ Discrepancy

The g factor of the magnetic moment of a particle describes the coupling between spin angular momentum and the magnetic moment of the particle. Dirac shows that this factor is $g = 2$ for the electron, and this would also extend to the muon. However, loop corrections can give an additional effect that was not taken into account by Dirac. Within the SM, it is expected that $a \equiv (g-2)/2 \neq 0$. If we examine the QED vertex, we can see that it can be expanded as the bare vertex plus higher order loop diagrams. One of these loop diagrams in particular corresponds to the magnetic moment being different than two and is seen in Fig. 2.1.

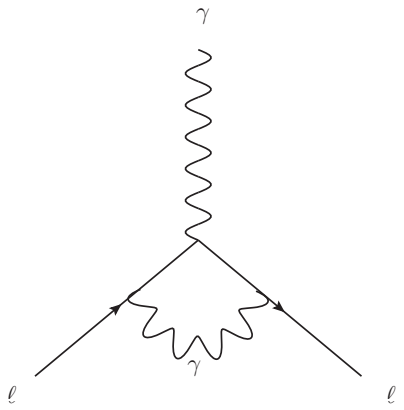

Figure 2.1: Single loop diagram contributing to the magnetic moment of the leptons.

This diagram, when computed for the electron, yields a contribution to $a_e \equiv (g_e - 2)/2 = \frac{\alpha}{2\pi}$. For the electron, this works very well and has precision down to 5 loops, which translates to 0.25 parts-per-billion [21]. This is actually used to do precision QED tests, and we take this to be how we define $1/\alpha = 137.035999174(35)$. The theory predicts $a_e = 1,159,652,181.78(77) \times 10^{-12}$, when using an alternative determination of α, as α is usually extracted by precision measurements of a_e.

However, this does not seem to work for the muon, or at least not as precisely as for the electron [22]. The value of $a_\mu \equiv \frac{(g_\mu - 2)}{2}$ was sought out at the Brookhaven E821 experiment in 2001, with their final result being delivered in 2004 [23]. They found that the true value is $a_\mu = 11,659,208.0(6.3) \times 10^{-10}$, yielding a difference of $\Delta a_\mu = (290 \pm 90) \times 10^{-11}$, a 3.4σ discrepancy between experiment and theory once the mass effects are taken into account [22]. Note that a_μ has many components contributing to it, and they can be split into the QED component, the EW component, and the hadronic component. The first two are known to very good accuracy, but the

hadronic component is naturally harder to compute. Once these are all taken into account at leading order and next to leading order, the expected theoretical value is $a_\mu = (11,659,180.4 \pm 5.1) \times 10^{-10}$. This strongly suggests that there is in fact a 3.4σ deviation.

While this discrepancy is not huge, and may still be the result of a statistical fluctuation or an error, it could be a window into new physics. Any new mediator that can be introduced in a loop similar to the loop diagram contributing to the magnetic moment and that couples to leptons will change a_μ and a_e. There is a wide variety of new physics options that have been investigated to solve the anomalous magnetic moment of the muon. For example, it has been speculated that weak scale physics, such as supersymmetric models with relatively light superpartners, could be responsible for the deviations in a_μ [24]. In particular, one model that has been examined quite extensively in this regard is the dark photon, which stipulates that the discrepancy arises from sub-GeV particles. The model allows for a region that could explain a_μ without disturbing a_e, since the mass may be too large to have an effect as a loop with electrons on the legs.

A recent effort at Fermilab has been taken to remeasure $(g-2)_\mu$ in the E989 experiment [25]. The expected result is a decrease in the uncertainty by a factor of four, reaching a precision of 0.14 ppm. There are also attempts to calculate a_μ more precisely with lattice QCD [26, 27, 28].

Chapter 3

Experiments

The intensity frontier may have means to access new light physics, even with extremely weak couplings to the SM. Many models involving new low mass states have been investigated at experiments at the intensity frontier, as the energy frontier typically is associated with a lower luminosity. B-factories have incredibly high collision rates. Belle, at the KEKB accelerator, has reached a total integrated luminosity of 1043 fb^{-1}, allowing one to probe small deviations from the SM in e^+e^- collisions. This also extends to decays, where experiments such as Mu3e will examine 10^{15} muon decays across the experiment's lifetime. Kaon decays are also explored at NA48/2 at the Super Proton Synchrotron (SPS) at CERN, which lives at an intersection of the energy and intensity frontiers, and has provided some 10^{11} kaon decays to study.

Adding a loosely coupled light particle can potentially add new decay modes with branching ratios $\propto \epsilon^2$, where ϵ is the coupling between the new physics and the SM. Most branching ratios are limited to be below 10^{-8} for new physics, with the mass of the mediators taken to be on the MeV scale. Limits from current experiments force one to accept either "dark" (*i.e.* weakly coupled) or heavy new physics. High luminosities and large numbers of decays provide a means to access the light, weakly coupled new physics.

This thesis is concerned with examining the existing and future sensitivity reach one can have with such models, at various experiments. By accessing different experiments, one can place limits for various ranges of the allowable masses. We will be looking at three physically different phenomenon across six experiments.

1. Mu3e is an experiment dedicated to looking at large numbers of muon decays, which allows limits on the mass range from $2m_e < m_\phi < m_\mu$.

2. NA48/2, and its successor NA62, provide access to many kaon decays, which will allow placing limits on the mass range from $2m_e < m_\phi < m_K - m_\mu$.

3. BaBar, Belle, and future experiment Belle2 use e^+e^- collisions near centre of mass energy of 10 GeV, considerably extending the reach in terms of the mass of the ϕ scalar to $2m_e < m_\phi < E_{\rm CM} - 2m_\mu$. Backgrounds can be expected to be better in the region of $m_\phi > 2m_\mu$.

Our final results will also include constraints from displaced decays at the beam dump experiment E137 conducted in the 1980's [29]. These computations are part of a work in progress [30]. As we will see in this chapter, many of our estimates will fail below 10 MeV. E137 is able to access low masses of the scalar and is able to place strong limits below 10 MeV, and so we can rely on its constraints in this range. Another beam dump experiment, E141, will be included in the final results, although these are weaker than E137 [31]. The results for E141 were obtained simply by scaling the dark photon limits to the scalar by identifying $e\epsilon = g_{\phi e}$, effectively identifying the production of the vector to be the same as the produciton of the scalar. One can do better than this, which will shift the E141 contours by an $\mathcal{O}(1)$ amount, which we ignore here. We will not discuss E137 or E141 further in this thesis.

3.1 Muon Decay at Mu3e

Mu3e [32] is a proposed experiment, currently under construction, that will look for the decay of $\mu^+ \to e^+e^+e^-$, which violates lepton flavour. This experiment will operate at PSI in Switzerland, and is currently taking data in its first phase for 2015-2016. A second phase for 2017 and beyond is planned, and the details of the phases are covered in this section. Lepton flavour violating (LFV) decays are allowed within the SM once one includes the neutrino masses. Since we see LFV processes in the neutrino sector, due to neutrino mixing, it is not unreasonable to expect that there may also be new physics that violates lepton number in the charged lepton sector. Mu3e is aiming to find Beyond the SM (BSM) LFV by investigating such μ^+ decays. The SM process for $\mu^+ \to e^+e^+e^-$ is shown in Fig. 3.1. For this process, the required neutrino oscillation that mediates the lepton flavour violating component suppresses the branching ratio of this process, so much so that $\mathrm{BR}(\mu^+ \to e^+e^+e^-) \ll 10^{-50}$. This is an unobservably low decay rate, and so any decays of this form will almost certainly be a sign for new physics.

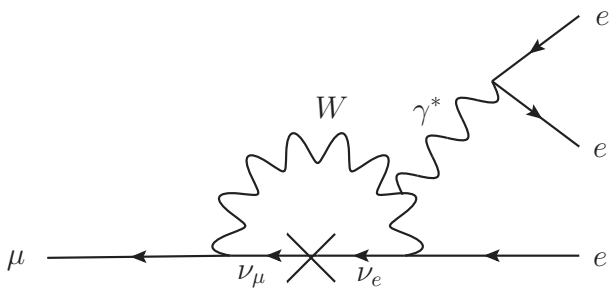

Figure 3.1: $\mu^+ \to e^+e^+e^-$ lepton flavour violating decay through a muon neutrino oscillating to an electron neutrino. This process is heavily suppressed due to the neutrino oscillation required.

New physics may come in the form of new particles that can mediate these loops without a penalty as seen in the neutrino mixing, if it is to be observed. This could be in the form of supersymmetric particles in a loop, or other particles which add couplings to muons and electrons. It is also possible that a new light mediator adds observable contributions at tree level.

The current experimental limits on the branching ratio of various flavour violating muon decay processes are shown in Table 3.1.

Decay Channel	Experiment	Branching Ratio	
$\mu \to e\gamma$	MEGA	$< 1.2 \times 10^{-11}$	[33]
	MEG	$< 2.4 \cdot 10^{-12}$	[34]
$\mu \to eee$	SINDRUM	$< 1.0 \times 10^{-12}$	[35]
$\mu\ Au \to e\ Au$	SINDRUM II	$< 7 \times 10^{-13}$	[36]

Table 3.1: Branching ratio limits on muon decay from various experiments as given in [32].

Note that all of these upper limits are on the order of $10^{-10} - 10^{-13}$. Any future experiments examining these decay modes must be sensitive to branching ratios at least as small as the upper limits here. For this reason, Mu3e is attempting to reach branching ratios down to 10^{-16} for the $\mu \to eee$ process. To reach such a low branching ratio, at least 5.5×10^{16} muon decays must be observed, if one assumes a total efficiency of 30%.

Given that this many muon decays are possible, the muon beam will be aimed at an aluminum target to stop the muons. The decay products of the muons are then tracked with the detector. A schematic of the target and the muon beam is shown in

Fig. 3.2.

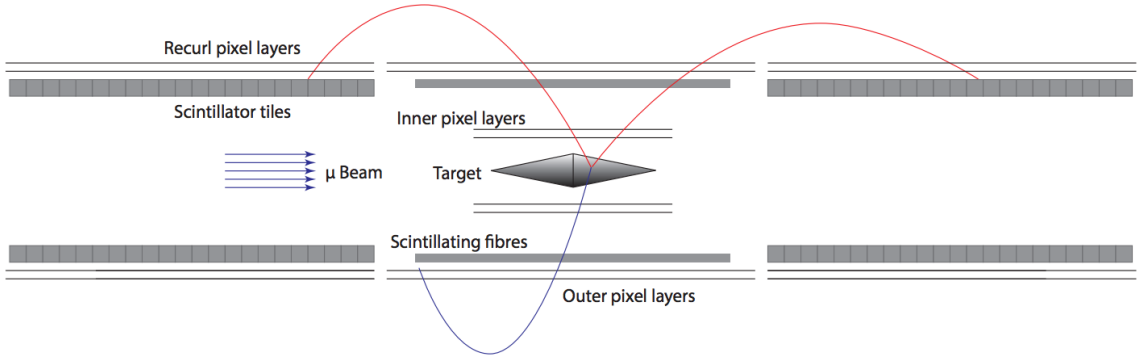

Figure 3.2: Schematic of a muon decay in the full Mu3e detector ready for phase II [32]. The cone-shaped aluminum target can be seen in the centre with two e^+ tracks curling upward in red, and an e^- track curling down in blue.

As we will see later in this section, the energy and momentum resolution of this experiment must be excellent for it to achieve the goals specified. This is because the SM process for $\mu^+ \to e^+\nu_e\bar{\nu_\mu}e^+e^-$ is much more frequent than the signal they are searching for, and rejecting this background is best done by enforcing momentum conservation to avoid missing energy in the final state. Having excellent energy and momentum resolution is also vital for the signal we will propose, as we must have good resolution on the invariant mass of an e^+e^- pair in the final state.

In order to achieve such a low sensitivity, and for practical purposes of building and commissioning the detector, Mu3e plans to run in two distinct phases of operation. The differences between these two phases lies primarily in the differences between the beam lines, which will be discussed below. There are also additions/modifications planned for the detector.

3.1.1 Phase I

The first phase will aim for a branching ratio sensitivity of 10^{-15}. PSI currently produces muons at a rate that Mu3e can take advantage of for the first phase, without modifications, and the first phase can additionally serve as a commissioning time. To produce the muons for the experiment, phase I will use the existing πE5 beam line. This is done by colliding protons on the target to produce pions. The proceeding strong interaction is given in equation 3.1.

$$p^+ + p^+ \to p^+ + n + \pi^+ \tag{3.1}$$

Note that this process is independent of the target Z since the interaction takes place directly between the proton beam and a single proton on the target. However, a carbon target is chosen due to, among other reasons, good heat dissipation, and its high density allows for a compact target with good pion production per unit volume. For production to be possible, the excess centre-of-mass energy must be at least as large as the pion mass, giving a threshold energy of 290 MeV for the proton beam. To obtain a reasonable yield of pions, a 590 MeV proton beam is used that produces low energy ($10 - 120$ MeV) pions. A beam current of 2.3mA will be used.

Pions that have stopped near the surface of the target give rise to surface muons, since the pion decays through the weak force to muons, as shown in equation 3.2.

$$\pi^+ \to \mu^+ + \nu_\mu \tag{3.2}$$

The pions have incredibly short lifetimes of 2.6×10^{-8} s, and the branching ratio of this process is very large: $\mathrm{BR}(\pi^+ \to \mu^+ + \nu_\mu) = 99.98770\%$ [37]. One does not have to wait long then to have a good source of surface muons. A number of 10^{15} muon decays can be expected during this phase. Since the decaying pions are at rest, and the muon has a mass very close to that of the pion, the muons are produced with momenta of 28 MeV. These are easy to collimate and provide a very monochromatic beam of muons, since only 10% of the surface muons can be used due to an angular selection. The collimated beam of positively charged muons is then directed to a target within a solenoidal magnetic field at a rate of 1×10^8 μ^+/s. A schematic of the beam line that produces the muon beam is shown in Fig. 3.3.

At this time, the detector is relatively minimal compared to the plan for the full run and is currently using a pixel-only detector. The target is surrounded with a set of inner and outer silicon pixel detectors, allowing the determination of momentum, vertex position, and decay time. Phase I is actually split into phase IA and phase IB; a detector upgrade will occur in phase IB. The silicon pixel detectors used in phase IA have relatively poor momentum and timing precision and are the main focus of the upgrades. Even so, phase IA will have sensitivity on the branching ratios down to $\mathcal{O}(10^{-14})$.

For phase IB, the first pair of recurl pixel layers will be added, along with the tile detectors and the fibre tracker. The recurl stations allow for the decay products to be seen as coming from outside the detector, as the radius of the charged decay products is typically larger than the detector. Improvements from adding the recurl stations

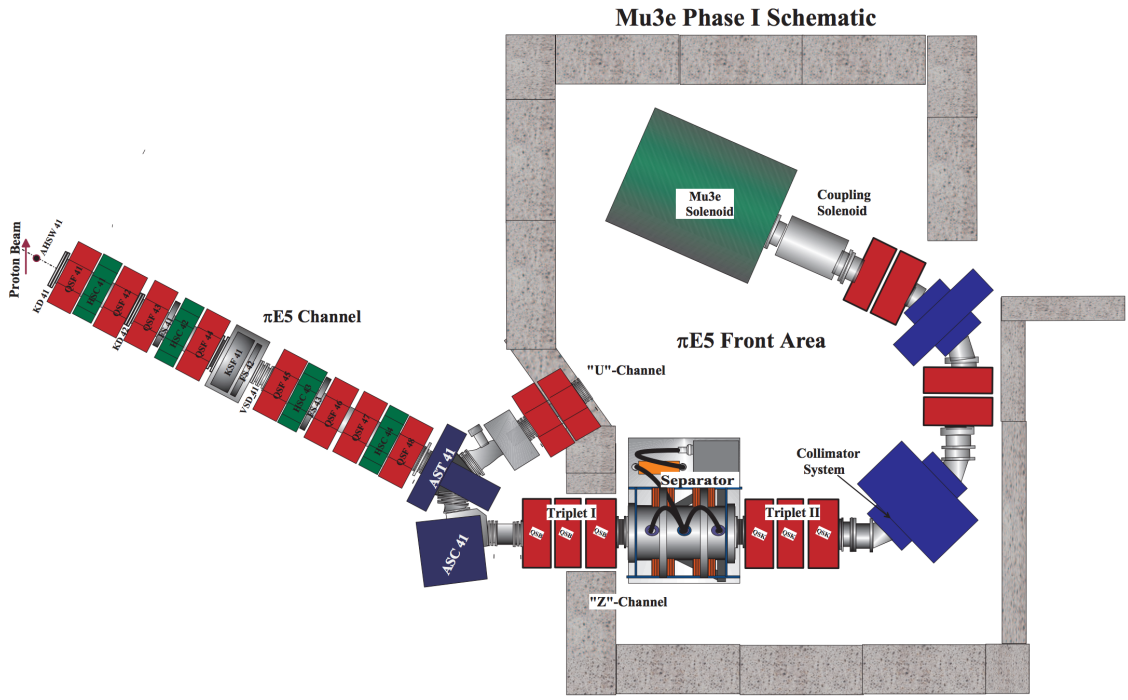

Figure 3.3: Mu3e phase I beam line schematic using the πE5 at PSI [32].

with the tile detectors allow for momentum resolution of 0.44 MeV. Similarly, the fibre tracker and tile detector also improve the timing resolution to $\mathcal{O}(100 - 300$ ps). It is also worth noting that the total energy resolution is less than 1 MeV.

3.1.2 Phase II

The largest difference between phase II and phase I is the upgrade planned for the beam line, where the πE5 muon beam will be replaced by the planned high-intensity muon beam (HiMB). The HiMB will work by taking advantage of the Swiss Spallation Neutron Source (SINQ) already in place at PSI.

Similarly to the πE5 beam, a proton beam strikes a target, however now the target is a spallation neutron source. As the protons strike the target, which is made of lead, zirconium, aluminum alloy, surface muons are created in the aluminum layer. The muons that are accessible are travelling in the opposite direction of the proton, such that even though they have the same sign charge, they can be separated by bending them in opposite directions, and a collimated beam of muons can be created. A diagram of the new beam line is shown in Fig. 3.4, where the Mu3e detector would be placed on the far side of the muon beam cellar.

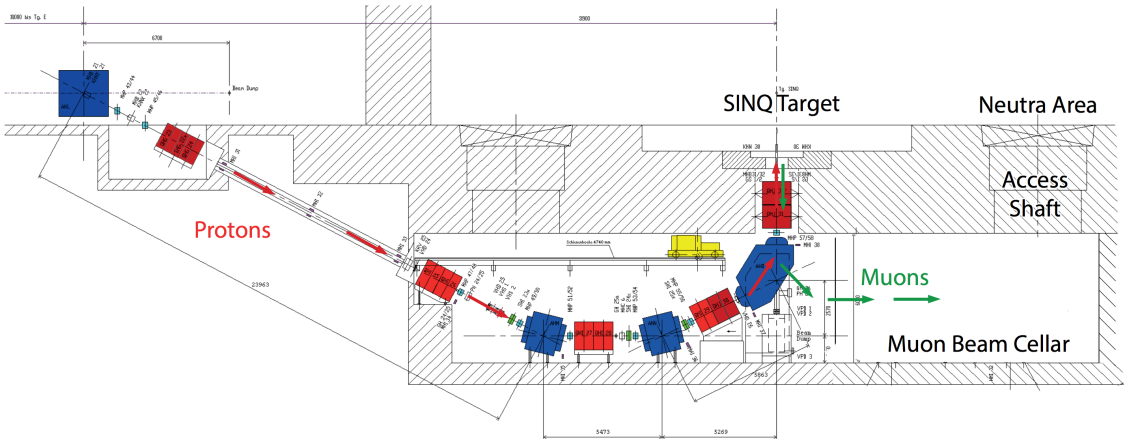

Figure 3.4: Mu3e phase II beam line schematic using the HiMB at PSI [32]. The Mu3e detector would be placed past the muon beam cellar. This production mechanism can allow for $\mathcal{O}(10^{10})$ μ^+/s decays.

Moving to the HiMB provides an estimated muon decay rate of 2×10^9 μ^+/s. To take advantage of the high-intensity beam, the detector will also receive an upgrade, where a second set of recurl stations will be added to further improve momentum resolution. This improves the momentum resolution to 0.28 MeV.

For all phases combined, the expected branching ratio sensitivities are shown in Fig. 3.5. Across the entire lifetime of the experiment, it is expected to see a total of 5.5×10^{16} muon decays for study.

3.2 Charged Kaon Decays at the Super Proton Synchrotron

NA48/2 [38] and NA62 [39] (also known as NA48/3) are two experiments studying rare kaon decays at the CERN SPS. Each experiment has its own objective, but both study kaon decays and have a dedicated K^+ beam, which we can take advantage of for the purpose of setting limits. Note that the beam is actually a simultaneous K^+ and K^- beam, but there are some advantages that make the K^+ beam more desirable. The charged kaon beam is produced similarly to the muon beam that was described in the previous section. Protons are collided with targets that produce a secondary beam, which are steered towards a target after being selected to ensure that the beam content is purely kaons. Beryllium is used as for the target, and the

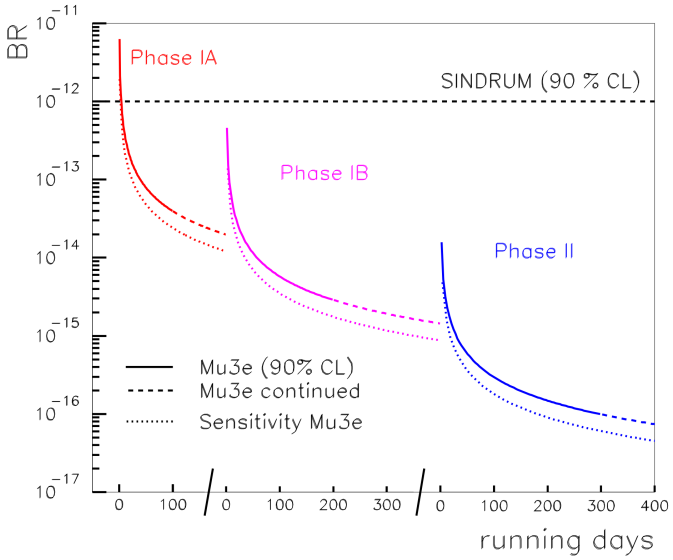

Figure 3.5: Expected branching ratio sensitivity for Mu3e [32]. Each phase can be seen to distinctively increase the sensitivity, with the target sensitivity being reached with the HiMB beam line upgrades and the two recurl stations with fibre tracker being added.

beam is a 400 GeV proton beam.

3.2.1 NA48/2

NA48/2 finished taking data in 2004, yet limits on new physics can still be derived using the data collected and stored on tape. NA48/2 is based on the upgraded NA48 experiment, and was primarily designed to look for charge-parity (CP) violation in the decays of charged kaons:

$$K^{\pm} \to \pi^{+} + \pi^{-} + \pi^{\pm} \tag{3.3}$$

$$K^{\pm} \to \pi^{0} + \pi^{0} + \pi^{\pm}. \tag{3.4}$$

The experiment collected 1.0×10^{11} K^{+} decays inside its fiducial volume during the running time from $2003 - 2004$. The data stored on tape is still being used to put some of the most competitive limits on the dark photon parameter space, and has recently ruled it out as a candidate for the resolution of the $(g-2)_{\mu}$ discrepancy [40]. For the majority of this analysis, we will be treating NA48/2 as the NA62 experiment with a scaled down number of kaons decaying in the fiducial volume.

3.2.2 NA62

NA62 is looking to measure the Cabbibo-Kobayashi-Maskawa (CKM) matrix element $|V_{td}|$ at the level of 10% by measuring the very rare charged kaon decay:

$$K^+ \to \pi^+ + \nu + \bar{\nu} \tag{3.5}$$

The SM branching ratio has been determined to be $\mathrm{BR}(K^+ \to \pi^+ + \nu + \bar{\nu}) = (7.81 \pm 0.75 \pm 0.29) \times 10^{-11}$, with the first uncertainty being due to the input parameters, and the second uncertainty coming from theory [41]. Precise measurements of this branching ratio should allow one to put strong limits on any new physics involving the charged kaons. In October 2014, NA62 successfully launched and began taking data. It is expected to collect 4.5×10^{12} K^+ decays within the fiducial volume for each year of running at the SPS.

Different than the previous experiments, NA62 is analyzing kaon decays while they are in flight 75 GeV K^+ beam. This beam momentum is well defined, having an error of 1%. The liquid krypton (LKr) electro-magnetic calorimeter is reused from the NA48 experiments and is placed past the fiducial volume, giving a coverage of 8.5 mrad from the beam. New to this experiment are the Muon Veto (MUV) and the Large-Angle Photon Vetoes (LAV). The LAV provides coverage from the LKr limit of 8.5 mrad up to 50 mrad, and has an inefficiency of $10^{-3} - 10^{-4}$ of detecting photons with energies down to 150 MeV. The MUV is used to reject muons, which is also handled by the Ring Imaging CHerenkov (RICH) detector. There are many other important components to the experiment, but the most important things that we must consider are the beam momentum, the LKr calorimeter, and the photon veto efficiency. To estimate relevant backgrounds, we need to know the probability of not detecting a photon, the probability that the events will hit the LKr calorimeter, and the energy resolution, which is quoted at

$$\frac{\sigma_E}{E} = \sqrt{\left(\frac{3.2\%}{E^{1/2}}\right)^2 + \left(\frac{9\%}{E}\right)^2 + (0.42\%)^2} \tag{3.6}$$

with E measured in GeV.

A schematic view of the experiment is laid out in Fig. 3.6.

One advantage to using a K^+ beam over a K^- beam is that the production rate is $K^+/K^- \approx 2.1$ higher for each 400 GeV proton striking the target, while the relative number of pions created which contaminate the beam compared to that of a K^- beam

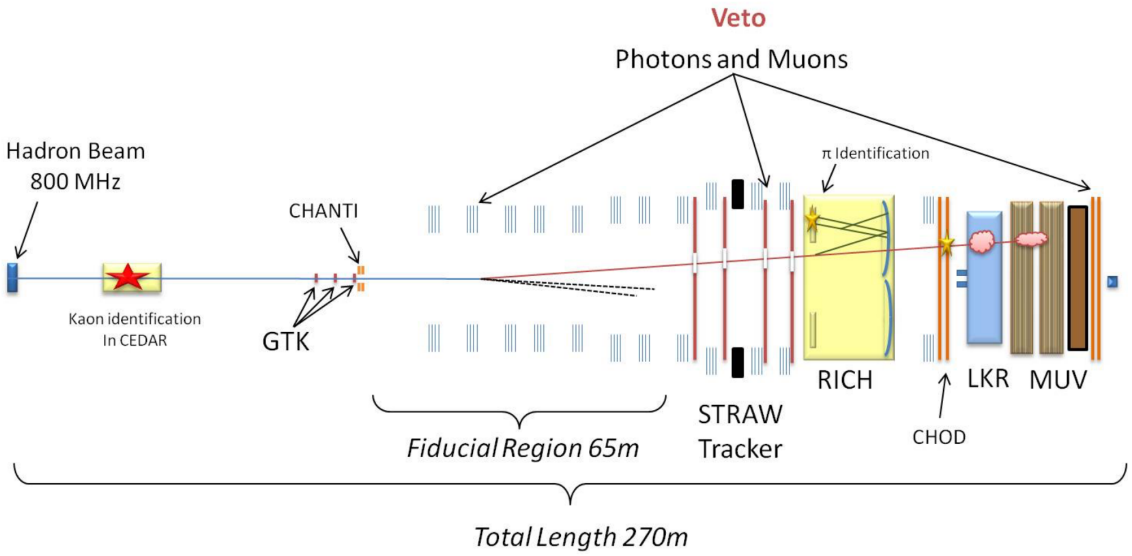

Figure 3.6: Schematic of the NA62 experiment from [39]. The beam collides with a beryllium target and kaons are identified. K^+ decays that are visible will decay within the fiducial volume and be captured by the LKr calorimeter. Beyond that, photons can be captured and vetoed outside of the calorimeter.

is only $(K^+/\pi^+)/(K^-/\pi^-) \approx 1.2$.

3.3 e^+e^- Collisions at B-factories

The B-factories BaBar [42], Belle [43], and the future experiment Belle2 [44] provide high intensity collisions while still reaching higher energies than typical meson decays have access to. These experiments are used to produce many B mesons by tuning the energy to the $\Upsilon(4S)$ resonance. The $\Upsilon(4S)$ is a $b\bar{b}$ quark bound state with a large preference to decay to B mesons, having a branching ratio > 0.96 [37]. For an e^+e^- collider of 3.5 GeV and 8 GeV respectively, the centre-of-mass energy is $\sim 2\sqrt{E_+E_-} = 10.58$ GeV; at this energy the $\Upsilon(4S)$ is just barely produced and must be at rest in the centre-of-mass frame. The KEKB collider provides high and low energy rings of electrons and positrons, called the HER and the LER, for the Belle experiment. SLAC provides the collider for the BaBar detector. It is important to note that the beam energies are asymmetric. This is to give any decay products a boost down the beam pipe before decaying, extending their lifetimes in the lab frame due to Lorentz time dilation. It also allows one to more clearly measure the vertex displacement from the production of the Υ to its decay point. To this end, the

detector is also built with this forward direction in mind. This energy just happens to be right above the threshold for a decay into a pair of B mesons, which have interesting properties to study. For instance, one can measure the amount of CP violation present in the $B/\bar{B}$ system. It is also possible to measure the neutral B meson oscillation into its anti-particle, $\bar{B}^0 \leftrightarrow B^0$. Measuring CP violation was the primary mission of the BaBar experiment. Over their lifetimes, when Belle ran from 1999-2010, Belle collected ~ 1000 fb^{-1} worth of data, and BaBar collected roughly half of this. The new experiment, Belle2, will be operating in conjunction with upgrades to the KEKB collider, where it will be rebranded as the SuperKEKB collider [45]. Commissioning for the new collider and detector upgrades begins in 2016. It is expected that 100 times the integrated luminosity in e^+e^- decays will be collected over its lifetime, reaching $\mathcal{O}(10-100)$ ab^{-1}. It will operate at the same centre of mass energy, but with less of a trade off to the asymmetry by using a 4 GeV positron beam and a 7 GeV electron beam.

In this work, these B-factories are interesting because they allow access to mediator masses up to ~ 10 GeV. Our model will couple leptons to a new scalar particle with a strength proportional to the mass of the lepton. In the other experiments discussed so far, Mu3e, NA48/2, and NA62, we were limited to couple to muons. However, at this scale, tau leptons are copiously produced with enough room in the phase space to still have associated emission of dark scalars. For our purposes of exploring the sensitivity reach, we will consider these three experiments to be the same, with a difference in the total integrated luminosity. We do not simulate the detector performance, which will be sufficient for this work. Another main reason why we target the BaBar and Belle experiments in this thesis is that there is already a lot of data taken on tape. BaBar and Belle blind their data during analysis, so unless the analysis is performed, it is not possible to know if there are any events present that correspond to our final state, $\tau^+\tau^-\phi,\ \phi \to \ell^+\ell^-$. Note that this also implies that any limits we place are merely potential limits on the sensitivity, not strict upper limits. Dedicated experimental analyses will be required to conduct the search of ϕ via the signature that we suggest.

Chapter 4

Analysis Framework

The aim of our analysis is to put limits on the experiments discussed earlier using our particular model. In order to do this, we will have to clearly define our model first. Then we will use an event generator, after which the final state of each event will be analyzed. From a phenomenological perspective, it is relatively easy to generate decay or collision events using modern tools, given a model's Lagrangian.

4.1 Models

Keeping in mind that the discrepancy of the proton-charge radius is about 4%, we must be interested in rather small couplings [13]. Our primary model of interest is the addition of a scalar, ϕ, with a weak, asymmetric coupling to leptons that violates lepton universality. We are also interested in the dark photon model, as it provides a similar low mass mediator that is weakly coupled to leptons. In the dark photon model, this is instead a vector as opposed to a scalar.

4.1.1 Dark Photon

The dark photon model adds a new $U(1)'$ force where the mediator now carries a mass. Giving the dark photon, known as A' (or alternatively the V), a kinetic mixing with the photon allows it to couple to charged particles with a coupling that depends on the mixing strength. This model has been thoroughly examined in the literature in connection with dark matter physics, and is a fairly general extension to the SM [46]. It also has potential to solve the $(g-2)_\mu$ problem [47], however, more recently

the parameter space for the simplest model has effectively closed off the dark photon as a solution to $(g-2)_\mu$ [48].

The simplest version of the dark photon Lagrangian is given below in equation 4.1:

$$\mathcal{L} = -\frac{1}{4}F'^2_{\mu\nu} + \frac{1}{2}m^2_{A'}A'^2_\mu - \frac{\epsilon}{2}F'_{\mu\nu}F^{\mu\nu} + \mathcal{L}_{\text{SM}} \tag{4.1}$$

Here $F'_{\mu\nu} \equiv \partial_\mu A'_\nu - \partial_\nu A'_\mu$ is the field strength tensor corresponding to the dark photon vector field A'_μ, $F_{\mu\nu}$ is the typical QED electromagnetic field strength tensor, $m_{A'}$ is the corresponding dark photon mass, and ϵ is the kinetic mixing strength. The mass term appearing here actually could be inserted from a new Higgs field breaking the $U(1)'$ symmetry, and the QED field strength tensor could be replaced with the $F^Y_{\mu\nu}$ tensor from the SM $U(1)^Y$ electroweak group. From a phenomenological point of view, it is sufficient to leave the mass term as it appears for our purposes.

After integrating the kinetic mixing term appearing in the Lagrangian by parts, the coupling to charged leptons (and quarks) becomes

$$\mathcal{L} \supset \epsilon A'_\mu J^\mu_{EM} \tag{4.2}$$

where $J^\mu_{EM} \equiv e\bar{\psi}\gamma^\mu\psi$ is the electromagnetic current. We then have a coupling between fermions and the dark photon with strength ϵe, *i.e.* it looks just like the typical QED coupling but suppressed by a factor of ϵ. Taking the dark photon to decay to SM particles, we have that the partial width of the dark photon to go to a lepton pair is given by,

$$\Gamma_{A'\to\ell^+\ell^-} = \frac{\alpha\epsilon^2}{3}m_{A'}\sqrt{1-\frac{4m^2_\ell}{m^2_{A'}}}\left(1+\frac{2m^2_\ell}{m^2_{A'}}\right) \tag{4.3}$$

which yields the convenient decay length when decaying to electrons to be given by [49],

$$c\tau_{A'\to e^+e^-} \approx 0.8 \text{ mm}\left(\frac{10^{-4}}{\epsilon}\right)^2\frac{10 \text{ MeV}}{m_{A'}}. \tag{4.4}$$

One can see that for small ϵ, the additional signature of the A' could be its displaced decay, away from the point where it has been produced.

In this model, the coupling to each lepton is the same. It is not immediately clear that one can have an asymmetric effect across leptons on the charged proton radius, or the magnetic moment. However, in the case where a muon is concerned,

the virtual particles may be much more massive. For this reason, the muon is much more sensitive to undiscovered particles, such as an A', than the electron, regardless of the couplings being the same between muon and electron. This minimal model proved sufficient for an explanation of $(g-2)_\mu$, but did not quite work for the proton radius anomaly. A plot of the current limits of the parameter space in ϵ^2 and $m_{A'}$ is shown in Fig. 4.1.

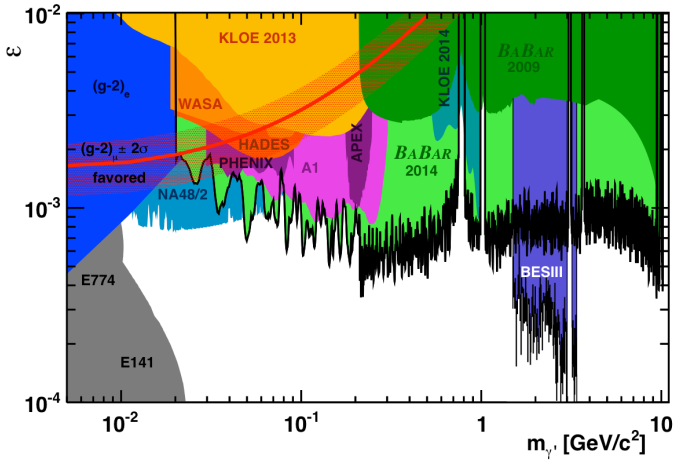

Figure 4.1: Current limits on the parameter space of the dark photon from [50]. The red band displays the region where the minimal dark photon model could explain $(g-2)_\mu$, and the dark blue region indicates the region ruled out by measurements of $(g-2)_e$. Recently NA48/2 has ruled out the possibility of the minimal model solving the anomalous magnetic moment of the muon.

4.1.2 Dark Scalar

The Lagrangian we use for the addition of a scalar will replicate some features of the Higgs' Lagrangian after electroweak symmetry breaking, which couples to leptons. We add a real scalar with Yukawa couplings to the three generations of mass, and a standard kinetic term, where the coupling strength is proportional to the mass of the lepton. This obviously requires picking a mass scale for the coupling, one of the two free parameters in the theory. The other free parameter is, of course, the mass of the new particle. Choosing the coupling to scale proportionally to the mass may give a natural way to couple the new scalar more strongly to the muon than for the

electron. The full Lagrangian is given below,

$$\mathcal{L} = \frac{1}{2}\partial_\mu\phi\partial^\mu\phi - \frac{1}{2}m_\phi^2\phi^2 + \sum_{\ell=e,\mu,\tau} g_{\phi\ell}\ \bar{\ell}^\lambda\ \phi\ \ell^\lambda + g_{\phi p}\ \bar{p}\ \phi\ p + \mathcal{L}_{\rm SM} \tag{4.5}$$

where ℓ takes on the lepton fields, $g_{\phi\ell}$ are the couplings between the scalar and the corresponding lepton, p is the proton field, $g_{\phi p}$ is the coupling between the scalar and the proton, and $\mathcal{L}_{\rm SM}$ is the SM Lagrangian. λ indicates spinor indices, and $g_{\phi\ell} \propto m_\ell$. We usually fix the coupling to the muon in this thesis, however we will also fix the coupling to the tau in one sectionso it is convenient to write the couplings as

$$g_{\phi\ell} = (g_{\phi e}, g_{\phi\mu}, g_{\phi\tau}) = g_{\phi\mu}\left(\frac{m_e}{m_\mu}, 1, \frac{m_\tau}{m_\mu}\right) = g_{\phi\tau}\left(\frac{m_e}{m_\tau}, \frac{m_\mu}{m_\tau}, 1\right). \tag{4.6}$$

It is important to point out that this Lagrangian does not possess $SU(2) \times U(1)$ gauge invariance, as Yukawa interactions with leptons explicitly break this gauge symmetry. This is a hint that this theory is not UV complete, and at best represents a low-energy limit of a more consistent theory. However, a UV complete version of this model, respecting $SU(2) \times U(1)$ gauge invariance, has been worked out that involves a SM neutral light scalar and a leptonic-specific two Higgs-doublet model [30].

With this model, the partial decay widths of the ϕ to a pair of leptons goes as

$$\Gamma_{\phi\to\ell^+\ell^-} = \frac{1}{8\pi}g_{\phi\ell}^2 m_\phi \left(1 - \frac{4m_\ell^2}{m_\phi^2}\right)^{\frac{3}{2}}. \tag{4.7}$$

Loop induced diagrams also allow the production of a pair of photons, $\phi \to \gamma\gamma$, which is computed with the diagram in Fig. 4.2.

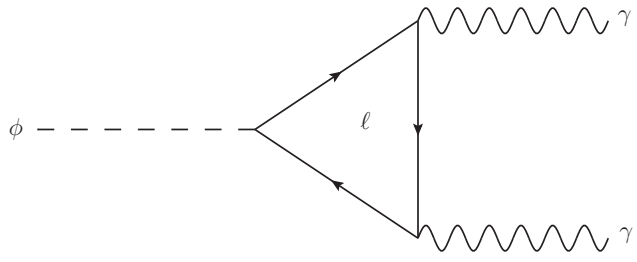

Figure 4.2: Loop diagram for $\phi \to \gamma\gamma$, mediated by an exchange of leptons.

This production has a small branching ratio, except for masses of the scalar near

the production threshold for a pair of muons of taus. Since ϕ is Higgs-like, we can make use of the known results for $\Gamma(H \to \gamma\gamma)$ in [51], and simply rescale the result to match our scalar. Doing this yields

$$\Gamma(\phi \to \gamma\gamma) = \frac{\alpha^2}{256\pi^3}\frac{m_\phi^3}{m_\mu^2} g_{\phi\mu}^2 \left(\sum_{\ell=\mu,\tau} \frac{2}{x_\ell^2} \left(x_\ell + (x_\ell - 1)\arcsin^2\left(\sqrt{x_\ell}\right)\right)\theta(1-x_\ell) \right)^2 \tag{4.8}$$

where $x_\ell = m_\phi^2/4m_\ell^2$, and $\theta(x)$ is the Heaviside step function. We do not take into account the resonant production of the leptons appearing in the diagram, hence the lack of electrons appearing in the sum, and the Heaviside function appearing to turn off the contribution above the resonant production threshold. At low masses of the ϕ, the contribution from both the muon and tau loop are identical, as we couple stronger to the more massive tau in such a way that both cases are identical. This correction is small in this region, compared to the partial width of $\phi \to e^+e^-$. However, near $m_\phi = 2m_\mu$, this process can have a branching ratio up to 20%. This is taken into account in our analysis by simply scaling the number of signal events by the correct branching ratio. It is possible to take this production of photons into account as a source of signal, and to include the appropriate backgrounds, but this is outside the scope of this work.

The largest implication of this decay width for us is the relative partial widths between muons and electrons as the decay products. Once the muon channel opens up, *i.e.* when $m_\phi > 2m_\mu \gg 2m_e$, and taking the total width to only have contributions from the e^+e^- and $\mu^+\mu^-$ channels, we have that

$$\mathrm{BR}(\phi \to \mu^+\mu^-) \approx \frac{1}{1 + \frac{\Gamma(\phi\to e^+e^-)}{\Gamma(\phi\to\mu^+\mu^-)}} \tag{4.9}$$

$$\frac{\Gamma_{\phi\to e^+e^-}}{\Gamma_{\phi\to\mu^+\mu^-}} \approx \frac{m_e^2}{m_\mu^2}\left(1 - \frac{4m_\mu^2}{m_\phi^2}\right)^{-\frac{3}{2}}. \tag{4.10}$$

Due to the suppression from the leading m_e^2/m_μ^2 term, once the decay to muons is kinematically accessible due to the large mass of the ϕ, one can effectively neglect the branching ratio to the electrons and take $\mathrm{BR}(\phi \to \mu^+\mu^-) \approx 1$. A plot of the branching ratio to a dimuon pair is shown in Fig. 4.3.

This has the consequence of allowing us to estimate sensitivity limits in an easier

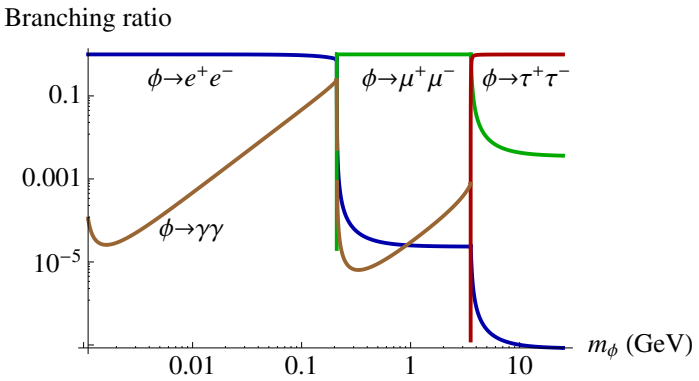

Figure 4.3: Branching ratios of the scalar to a pair of leptons or to a pair of photons. Blue corresponds to $\phi \to e^+e^-$, green to $\phi \to \mu^+\mu^-$, red to $\phi \to \tau^+\tau^-$, and brown to $\phi \to \gamma\gamma$. Going slightly above the threshold mass to produce pairs of muons gives a branching ratio of 1 almost immediately. Note the contribution from the loop induced production of photons is appreciable just to the left of $m_\phi = 2m_\mu$.

fashion, as we need only take into account the electron decay channel and photon production channel, until the muon is accessible (where it dominates), and similarly for the tau. In all of our cases, we will be taking the ϕ to be produced on-shell before decaying to an $\ell^+\ell^-$ pair promptly, as the width of the scalar as given above is very small, and the branching ratio to the most massive pair of leptons is very close to 1.

If we examine the decay length, where the electron is the only accessible lepton and for masses of the mediator much larger than the electron, we find

$$c\tau_{\phi\to e^+e^-} \approx 0.05 \text{ mm} \left(\frac{10^{-4}}{g_{\phi e}}\right)^2 \frac{10 \text{ MeV}}{m_\phi}. \tag{4.11}$$

The decay length is plotted in Fig. 4.4.

Of most importance is the relative magnitude of the couplings. We would like a weak coupling to electrons such that we do not disturb the proton radius as extracted in the electron-proton scattering experiments, and in measurements of the atomic energy levels of electronic Hydrogen. Indeed the point here is to have a stronger coupling to the muon with the scalar than that of the electron with the scalar. Taking the couplings to be Higgs-like gives the size of any physical effect to be approximately some power of $(m_\mu/m_e) \approx 210$ times larger for the muon than to the electron. Therefore, it is advantageous to produce such a scalar by radiating it off of the heaviest lepton kinematically accessible in any given process.

It is also possible to allow for a pseudo-scalar coupling to be included by intro-

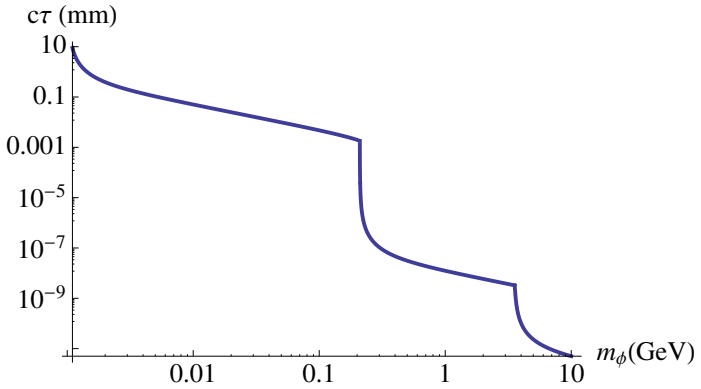

Figure 4.4: The typical decay length of the scalar. The strength of the coupling between ϕ and the electron is taken to be $g_{\phi e} = 10^{-4}$. One can see the different decay modes turn on, at the $2m_\mu$ and $2m_\tau$ thresholds, while the effects due to the loop diagram $\phi \to \gamma\gamma$ do not have a sizable impact on the decay length.

ducing another set of couplings to the pseudo-scalar field with an $i\gamma^5$ between the spinors. While it is outside the scope of this thesis to examine this, we will note here that the scalar and pseudo-scalar have corrections to $(g-2)_\mu$ with opposing signs. This is given in more detail in [13].

Since the phenomena we are trying to describe are the anomalous magnetic moment of the muon and the muonic atom's Lamb shift, we will discuss how the scalar model modifies these in detail. The corrections to $(g-2)_\mu$ are given at the one loop level by [52, 53, 54]. A convenient form for the contribution from the addition of a scalar is given below.

$$\Delta a_\mu = \frac{\alpha}{2\pi}\left(\frac{g_{\phi\mu}}{e}\right)^2 \xi\left(\frac{m_\phi}{m_\mu}\right) \tag{4.12}$$

$$\xi(x) = \int_0^1 \frac{(1-z)^2(1+z)}{(1-z)^2 + x^2 z}\, dz \tag{4.13}$$

This form of Δa_μ will be useful when plotting our proposed sensitivity limits. For the case where $m_\phi \ll m_\mu$, the integral $\xi \to 3/2$, giving an m_ϕ independent constraint on the coupling constant in this region. When we are in the region where $m_\phi \gg m_\mu$, the contribution at one loop scales as $\Delta a_\mu \propto (m_\mu/m_\phi)^2$, or similarly, the constraining coupling must scale as $g_{\phi\mu} \propto m_\phi/m_\mu$. Overall we have the following asymptotic behaviour:

$$\Delta a_\mu = \frac{\alpha}{2\pi}\left(\frac{g_{\phi\mu}}{e}\right)^2 \begin{cases} \frac{3}{2}, & m_\phi \ll m_\mu \\ \frac{m_\mu^2}{m_\phi^2}\left(2\ln\left(\frac{m_\phi}{m_\mu}\right) - \frac{7}{6}\right), & m_\phi \gg m_\mu \end{cases}, \tag{4.14}$$

and at a specific mass

$$\Delta a_\mu\left(m_\phi = 50\text{ MeV}\right) = \frac{\alpha}{2\pi}\left(\frac{g_{\phi\mu}}{10^{-4}}\right)^2 8.6\times 10^{-8}. \tag{4.15}$$

The muonic atom's Lamb shift correction from the addition of a scalar can be found through first-order perturbation theory, and is given by [54, 13]

$$\delta E_\phi = \int r^2 V_\phi(r)\left(|R_{20}(r)|^2 - |R_{21}(r)|^2\right)\, dr \tag{4.16}$$

$$= \frac{\alpha}{2a^3}\left(\frac{g_{\phi\mu}g_{\phi p}}{e^2}\right)\frac{f(am_\phi)}{m_\phi^2}, \tag{4.17}$$

where $f(x) = x^4/(1+x)^4$, $a = 1/(\alpha m_{\mu p})$ is the Bohr radius of the μH system, and $m_{\mu p}$ is the reduced mass of the system. While this correction has proven to be a good motivation, and one can extract expected sensitivities from it with a constraint from the measurement of r_p, there is still a degeneracy in this expression that proves difficult to work around. Since the coupling to the proton must be included, we only see the product $g_{\phi\mu}g_{\phi p}$ enter in the above expression, which makes it difficult to place sensitivity limits on $g_{\phi\mu}$ without making assumptions on the coupling to the proton. For this reason, $(g-2)_\mu$ proves to provide better context for the sensitivity limits we will explore. We will still present the contours that yield the correct r_p in the final results for a few choices of a fixed coupling to the proton.

4.2 Event Generation

In order to understand the limits we want to impose on the parameters of our model, we must generate decay (or collision) events corresponding to each process which contributes to the final state. This also requires that we simulate appropriate background processes which can masquerade as signal. To achieve this, one has to integrate the square of the sum of each matrix element for a given process. In some cases, such as kaon decay which we will compute later, this is possible to do by hand, at least to some approximation. However, while the matrix elements are easy to write down,

usually these processes can be quite tedious and very difficult to integrate. For these cases, we will make use of *event generators*, which effectively sample the allowed phase space of the matrix elements by Monte Carlo in order to perform the integration.

Our primary tools we use are FeynRules [55], FeynCalc [56], and MadGraph5_aMC@NLO [57, 58]. FeynRules allows one to easily write down a Lagrangian and generate the Feynman rules dynamically. For our purposes, the Feynman rules are easily seen directly from the Lagrangian. However, the advantage of using FeynRules is that the output follows the Universal FeynRules Output (UFO) [59], and defining the model involves only writing some rather simple Mathematica code. The UFO defines a portable format for a model, allowing multiple event generators to utilize its output. MadGraph can utilize the resulting model simply by putting the UFO model into the appropriate location within MadGraph. FeynCalc is useful when assisting computations by hand, which is ultimately used for computing traces of many γ matrices.

There are other tools that could further improve our limits which were not used. These include PYTHIA [60], which would handle the hard event generation in place of MadGraph, hadronization (which is not likely to be of use here), initial and final state radiation; and Delphes [61], providing a proper detector simulation at a level that is not as demanding as Geant4 [62]. For our purposes of simply estimating limits, these are for the most part not necessary.

4.2.1 FeynRules

FeynRules was developed as a toolkit to define new fields, write down a given model's Lagrangian, and automatically compute the Feynman rules. The only requirements of the model are that the Lagrangian satisfy locality as well as Lorentz and Gauge invariance, and allowable fields have spin 0, 1/2, 1, 3/2, or 2. The Lagrangian need not be an extension of the Standard Model, but simply any quantum field theory obeying the above requirements. FeynRules will also analytically compute simple decay widths for $1 \to 2$ processes and branching ratios. This toolkit works as a Mathematica package.

Within a Mathematica notebook, we simply write down the Lagrangian in terms of the fields and request that the Feynman rules be calculated and written in the UFO format with the `WriteUFO[L + LSM]` command. Note that FeynRules contains the SM Lagrangian already, so we simply need to append our new La-

grangian to this built-in one. At the same time we have FeynRules calculate the decay widths of each new particle, and update the model file with these using the calls `vertices = FeynmanRules[L]`, `decays = ComputeWidths[vertices]`, and `UpdateWidths[decays]`.

Our model files for both the scalar and dark photon models are included in appendix A, and are the only input into the generation of our events besides the definition of the process of interest.

4.2.2 FeynCalc

Only used minimally in this thesis, FeynCalc provides a quick sanity check for calculations done by hand. We have used FeynCalc in our calculation of K^+ decays with new physics, although this channel is doable by hand. It is useful in two ways: first, it computes the traces of many γ matrices. For our purposes, a trace of only up to 6 γ matrices appeared (both with and without a γ^5 component). Second, one can also start from the amplitude as written with spinors, and FeynCalc can automatically write down the spin-averaged amplitude after taking the traces.

4.2.3 MadGraph

MadGraph is the largest component and most used tool of this thesis. It provides the framework for:

- Importing both the SM and new physics models as provided by tools such as FeynRules in the UFO format
- Defining processes of interest, such as $e^+e^- \to \mu^+\mu^-\mu^+\mu^-$
- Producing Feynman diagrams for the process automatically using the Feynman rules defined by the model
- Generating events by sampling the amplitude using a Monte Carlo technique

Note that while MadGraph is usually used for collider scenarios where the physics object of interest is the cross-section, it is also possible to use it to compute partial decay widths. This is useful when there are more than three decay products in the final state. For two decay products, the derivation of the decay width is trivial. When one moves to three decay products, the final state integration may

become tricky, but with a change of variables to any of the two invariant mass pairs, the integration can usually be done analytically, or at least numerically. This change of variables is usually used in so-called "Dalitz plots," where the phase space can be more easily visualized [37]. Beyond three decay products, the final state integration becomes increasingly difficult, and this is where we put MadGraph to use. Note that it is possible to extend Dalitz plots to four-body decays, but this is outside the scope of this thesis [63].

In our work, partial decay widths calculated by MadGraph are used for corrections to the μ^+ decay at the Mu3e experiment. While it would be possible to leverage MadGraph for calculations of the new physics component to the $K^\pm$ decay, we are only interested in the three-body decay where it is possible to do this analytically.

As is the case with any Feynman diagram calculation, any width or cross-section computation must include all relevant Feynman diagrams. MadGraph automatically will generate these given the Feynman rules defined, taking into account restrictions placed by the user, such as restricting a certain particle to be produced on-shell before decaying. Diagrams are generated efficiently by recursively merging sub-diagrams. Production of Feynman diagrams starts by treating all incoming particles as outgoing antiparticles. This simplifies the diagram generation and is easy to reverse as a final step. Next, all particles are grouped, with the maximum group size being the maximum degree of interaction, and replacing each group with its resulting particle if applicable, else it is discarded. Generation halts when at most two external particles remain, corresponding to the requirement that the particles must interact. This process results in all Feynman diagrams being produced that are allowed, by descending down through the tree of allowed diagrams and pruning branches early if they will not lead to the final state desired. A user can also request the maximum degree of interaction allowed. For example, we could require `QED=0` to allow only QCD interactions in the diagrams.

Once diagrams are generated, the amplitudes must be written down. This is done using helicity amplitudes. MadGraph passes this work off to an external library, either HELAS [64] or ALOHA [65]. Each external leg gets assigned a wavefunction, and is combined using the appropriate propagator until the final combination step gives the resulting helicity amplitude for that particular diagram. This also allows efficient generation as common sub-processes within a diagram can be reused across all Feynman diagrams.

Finally, the Monte Carlo integration takes place, where the objective is to integrate

the square of each combination of helicity amplitudes. MadGraph is composed of a few distinct tools, the most important of which is MadEvent. MadEvent is one of a few programs included in MadGraph that can sample a generated amplitude using Monte Carlo. Other Monte Carlo integrators could be used instead, such as PYTHIA, however MadEvent comes bundled with MadGraph. The parameters that one can tune for the generation of events falls under two files, labelled cards: `param_card`, and `run_card`. The `param_card` controls physics parameters, such as the mass of various particles and their couplings, both for the SM and any new physics models. `run_card` controls parameters related to the experiment, such as the energies of the particles being collided, which parton distribution functions to use, and any relevant cuts to make at generation time.

By changing the physics parameters for our new model, we can scan the parameter space allowed. For our purposes, the scaling of the relevant cross-sections and partial decay widths with the coupling $g_{\phi\ell}$ is straightforward. This is not the case with the mass of the scalar, and we have written a Python package that can generate MadGraph output as it scans across the mass regime of interest.

The output of the Python package is a metadata file containing the appropriate inputs to MadGraph, such as the `run_card`, `param_card`, model information, generated processes, and the resulting partial decay width or cross-section. Also included is an XML-like file containing all the events generated by MadGraph. This output follows the Les Houches Event file format[66], which acts as a standard way of representing particle decay/collision events. Each event entry contains a list of particles, and for each particle we are given the particle ID, the mother particle if it is a decay product, the colour(s), four-momentum, mass, proper lifetime, and spin, and a few other quantities not of relevance here. The XML-like structure translates nicely into a Mathematica style table. To import the events into Mathematica for analysis, a Mathematica package developed by Maxim Perlstein and Andi Weiler is used [67].

4.3 Extracting Sensitivity Limits

In this section we will detail the precise procedure used to set limits on the various experiments we have analyzed.

For the general case, we must generate the mass distribution for the signal and background processes of interest. We can do this by hand for the simpler cases, or using MadGraph to handle the sampling of the amplitudes for us. Once we have the

background and signal spectra, we must bin the events in the invariant mass of the outgoing lepton pair $m_{\ell\ell}$, based upon the appropriate detector's energy resolution. Additionally, we need to correct for any efficiencies that appear in detecting the final state of interest, such as angular acceptance.

Many fewer events are generated than the number of actual events expected to be observed. This is due to the amount of computing time required to sample events. With our current resources, generating $10,000$ events takes on the order of 15 minutes, while we expect to observe 10^{10} events or more in some cases. Clearly, we must then sample a smaller number of events, and then scale up our results to the appropriate integrated luminosity or number of total decays expected. This has an effect when using MadGraph to sample regions of the parameter space that are suppressed, especially near the tails of the background distributions, where only 0 or 1 events will be seen. Scaling these regions is hence not straightforward, however it is still the case that any signal in the tails of background distributions must be relatively easy to spot.

Note that because we are only predicting an expected limit for the experiments, we will likely err on the optimistic side for the number of signal events. However, if one were to actually look at the data from the experiments, the limit setting procedure must be precisely defined and all applicable efficiencies and backgrounds taken into account. This is best done by experimental collaborations.

For our scalar model, all processes of interest scale as $g_{\phi\ell}^2$. If we overlay the signal and the background binned in $m_{\ell\ell}$, we can look for the location of a bump due to the resonant production of the scalar propagator going on-shell. Scaling the strength of the signal by tuning $g_{\phi\ell}$ until we can claim the bump is statistically significant yields a limit on the coupling constant for that choice of m_ϕ. Assuming Poisson statistics in each bin, we choose our limit such that the signal is a 3σ effect; *i.e.* $S = 3\sqrt{B}$ with S being the number of signal events and B being the number of background events.

We can use the fact that we know how the signal scales with our coupling when generating events with MadGraph. To produce events at a faster computational rate, we set the coupling to 1 since it will be rescaled later when taking the limit. Reducing the coupling strength to a more reasonable value, such as 10^{-4}, will drastically increase the time taken to generate signal events. This is akin to having a very small allowable phase space when sampling with Monte Carlo.

Chapter 5

Results

In the last chapter, we detailed how we go about deriving sensitivity limits on the physics parameters in our scalar theory, from how we generate the raw events to extracting the upper bound on the coupling strength. Here we will present our results, as the limits on the coupling as a function of mass for a new scalar particle, for the various experiments discussed previously. This goes over the entire parameter space of $2m_e < m_\phi < (\sqrt{S_{\text{Belle2}}} - 2m_\tau)$, with different experiments taking different ranges of this total region. It is possible to go to even higher energies if we were to consider final states with four muons for the e^+e^- scenario, however we do not investigate this possibility further. For two of the experimental cases, we have used MadGraph Monte Carlo techniques, and for the third case we've been able to analytically solve for the limits. For all cases, our limits are at 3σ, as detailed in the previous section. What we will plot below is the solution, $g_{\phi\mu}$, to the equation $S(m_\phi, g_{\phi\ell})/3\sqrt{B} = 1$, with $S \propto g^2_{\phi\mu}$, with the number of signal and background events being defined by the Monte Carlo or our hand calculations. Specifically, since we know the scaling of the number of signal events (with each signal being defined in more detail below), we are solving the equation

$$g^{\text{limit}}_{\phi\mu} = g^{\text{test}}_{\phi\mu} \left(\frac{S(m_\phi, g^{\text{test}}_{\phi\ell})}{3\sqrt{B}} \right)^{-1/2} \tag{5.1}$$

for many masses over the parameter space, where $g^{\text{test}}_{\phi\ell}$ is the appropriate input coupling used to generate the events. This usually takes on a value of $0.1 - 1$. Note that the form of the limit given in equation 5.1 will vary from experiment to experiment, as we take into account various quantities such as signal efficiency, however we will always end up solving this same equation.

5.1 Limits from Muon Decays in Mu3e Experiment

In section 3.1, we saw how the production rate of μ^+ at Mu3e could be brought to the level of muon decays occurring at a rate $\mathcal{O}(10^9)$ μ^+/s. The signal for the Mu3e experiment, $\mu^+ \to e^+e^+e^-$, contains no missing energy as there are no neutrinos in the final state. The SM has many avenues to produce such a signal with missing energy through muon decay, and we will go through the relevant backgrounds for our sensitivity limits here. Since the experiment consists of many muons stopped in a target, it can be expected that there will be many events that behave like a muon decay and have missing energy. Our signal will overlap with the backgrounds present and Mu3e, and will allow us to study the signal component of $\mu^+ \to e^+\bar{\nu}_\mu\nu_e e^+e^-$.

For this experiment, we have utilized MadGraph to do the final state integration, as our signal will have five particles in the final state. Although only four must be integrated over as the ϕ is produced on-shell, this integration is difficult to do by hand. Furthermore, even though we will be looking at a four body decay, the scalar particle will be on-shell and decay later to an e^+e^- pair, and MadGraph will also take care of generating the events corresponding to this decay. All of the diagrams that MadGraph generates are available in appendix B.1.

5.1.1 Backgrounds

Here we will discuss the relevant backgrounds to the proposed signature and their implications/effects on our sensitivity limits.

A large irreducible background for the experiment is

$$\mu^+ \to e^+ + \bar{\nu}_\mu + \nu_e + e^+ + e^- \tag{5.2}$$

which comes with a branching ratio of 3.4×10^{-5} [37]. This is due to an internal conversion of muon to electron with a weak vertex, just like an ordinary muon decay (also known as a Michel decay.) To remove this background process, momentum conservation can be applied provided that the energy resolution is small enough. For Mu3e, a total energy resolution of $\sigma_E < 1$ MeV is sufficient for sensitivity of branching ratios down to 10^{-15} [32]. One such diagram for this process is shown in Fig. 5.1.

Another source of background for the experiment is the radiative muon decay

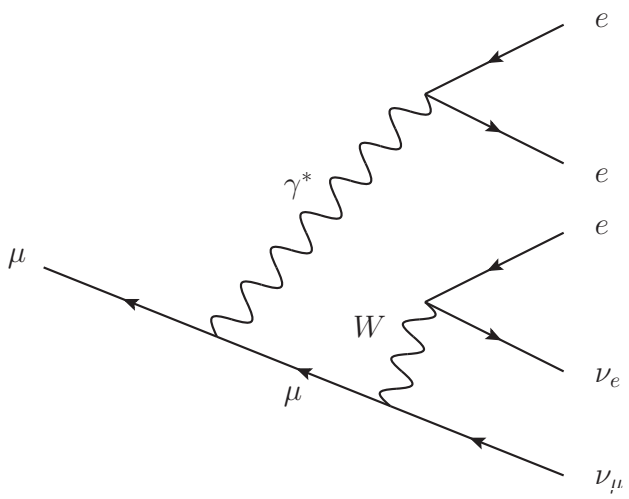

Figure 5.1: One Feynman diagram for the SM process $\mu^+ \to e^+\bar{\nu}_\mu\nu_e e^+e^-$. Here a virtual photon is emitted and decays to an e^+e^- pair. Note that the photon can be radiated off of any of the charged particles in the diagram before the e^+e^- decay. This background process can be suppressed by using momentum conservation with a high energy resolution.

$$\mu^+ \to e^+ + \bar{\nu}_\mu + \nu_e + \gamma \tag{5.3}$$

where the γ radiates off of either the muon or electron. This process comes with a branching ratio of 1.4×10^{-2}, given a photon energy larger than 10 MeV [37]. The photon can then convert to an e^+e^- pair in the detector or target material and mimic the irreducible background above. Conversions outside of the target can be suppressed if the vertex can be readily identified. This conversion process will be a much more important source of background for the low mass range of the scalar, as the e^+e^- pair from the converted photon will be highly collimated for all but the lowest photon energies. Within the target, this background appears as an accidental background with a regular muon decay.

There are other sources of background present as well. We have already briefly mentioned Michel decays, which can be identified by the lack of any negatively charged particle tracks, since the experiment uses a μ^+ beam. Bhabha scattering from the positrons coming from either the muon decay or a contaminated beam, scattering off of the target material to make an e^+e^- pair appear from a single vertex. This process has missing energy from the unaccounted electron in the target material and can be removed similarly to the irreducible background. Finally, there are also pions that

may contaminate the beam and decay either to $\pi^+ \to e^+e^+e^-\nu_e$, or $\pi^+ \to \mu^+\nu_\mu\gamma$ with the photon converting to an e^+e^- pair, which have branching ratios 3.2×10^{-9} and 2.00×10^{-4} relatively [37]. It is expected that the pion contamination is on the order of 10^{-12} for the HiMB [32], and the small decay rates should also suppress these numbers of events to safely negligible rates.

Using MadGraph, we generate $200,000$ events corresponding to the SM background for our signal, $\mu^+ \to e^+\bar{\nu}_\mu\nu_e e^+e^-$. We use such a high amount to have properly populated bins near the tails of the distribution, where the likelihood that a bin will be populated is small. To improve the time required to generate the events, we ignore contributions from the Higgs and the Z bosons, as they will not contribute at energies associated with muon decay. As a cross-check, the total width we obtain from the SM process is 1.239×10^{-23} GeV, yielding a branching ratio of 4.119×10^{-5}, which is within errors of the PDG value of $(3.4 \pm 0.4) \times 10^{-5}$ [37].

5.1.2 Signal

The signal we are interested in is the spectral feature over the irreducible background present in Mu3e. That is, the process we are investigating has the same final state as $\mu^+ \to e^+\bar{\nu}_\mu\nu_e e^+e^-$, but with the electron and one of the positrons reconstructing the mass of the scalar.

We will be using both the scalar model and the dark photon model here. The signal processes of interest are the decay chains

$$\mu^+ \to e^+ + \bar{\nu}_\mu + \nu_e + \phi,\ \phi \to e^+ + e^- \tag{5.4}$$

$$\mu^+ \to e^+ + \bar{\nu}_\mu + \nu_e + A',\ A' \to e^+ + e^- \tag{5.5}$$

with the ϕ and A' being produced on-shell. One diagram for the scalar case can be seen in Fig. 5.2. All of the diagrams generated by MadGraph that are used can be seen in appendix B.1. Note that while we generate events with the scalar radiating off of either the decaying muon or the positron from the muon decay, the emission from the muon dominates, unlike the QED case, due to the stronger coupling to the muon than the positron.

We generate events at $10,000$ events at 200 different mass points, logarithmically spaced from 1.1 MeV, slightly higher than $2m_e$, up to 100 MeV, slightly lower than m_μ.

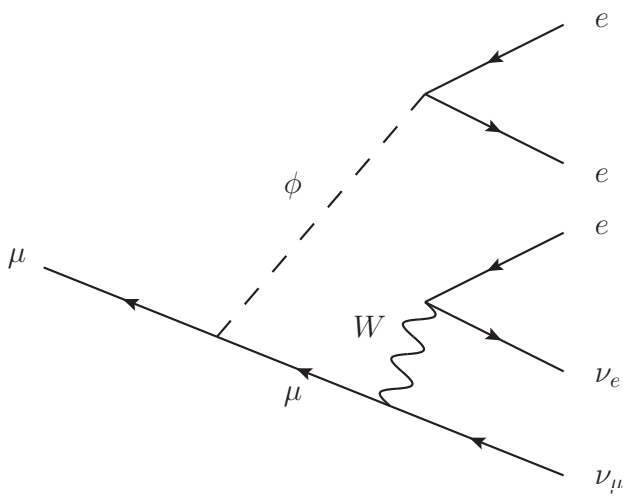

Figure 5.2: Feynman diagram for the scalar signal in muon decay. Remember that the scalar is produced on-shell here and can only decay to the e^+e^- pair.There is a second diagram with the scalar being radiated off of the electron from the W decay instead of off the initial state muon, however the emission off of the muon dominates. Two identical diagrams exist for the dark photon, where the A' replaces the ϕ.

It's worth briefly noting here that MadGraph does not natively support scanning over a parameter, such as the mass of the mediator. To get around this, we have written a wrapper around MadGraph in `Python`, which will directly interface with the MadGraph calls and can automatically run the generator over any parameter scan, with minimal overhead. For all runs, the coupling to the muon and scalar is set at $g_{\phi\mu} = 0.1$, and will be rescaled later to determine the limiting value. $10,000$ events were chosen to be generated to reduce the statistical error in each bin, as we will be scaling the number of events up to $\sim 10^{16}$ total events. This was also a sweet spot where the time taken to generate the events on a modern laptop was on the order of a few hours. The results of generating these events are twofold:

- The total width of the process is given, which we can use to rescale the events. For example,

$$\Gamma(m_\phi \approx 21 \text{ MeV}) = 1.3 \times 10^{-11}\ \Gamma(\mu^+ \to \text{all}) \left(\frac{g_{\phi\mu}}{10^{-4}}\right)^2. \tag{5.6}$$

  MadGraph tallies this partial width for us. This will capture the overall behaviour of our signal, corresponding to the total number of raw signal events all placed into one bin.

- A collection of events with the four-momentum for each particle, and their parents if they are a decay product are output by the program. We can use these to plot the spectrum of the decay products.

Once we have a collection of events, we can bin the results in a relevant parameter and use the spectrum to place limits on the sensitivity of Mu3e. A natural choice here is to plot the histogram of events in the invariant mass of the e^+e^- pair. Since the scalar is decaying on-shell and has a narrow width, the invariant mass of its decay products must equal the mass of the parent. This yields a resonant "bump" in the decay spectrum at the mass of the scalar, and the signal spectrum behaves as a delta-function. In reality, of course, this delta-function will be broadened by *e.g.* detector resolution. Since the final state has two positrons, it is not clear which to use when constructing the invariant mass spectrum. These should be back to back, but only in the rest frame of the scalar, so that there are no obvious selection cuts one can apply on an event-by-event level. However, for our simple analysis, we construct both available pairs and simply correct by a factor of two. Note that while we know the true parent particle, we do not make use of this information to better reflect an experimental search for the scalar.

The choice of binning is very important. If they are too wide, the signal features can be spread across a wide number of background events in the same bin. On the other hand, we are limited by the detector's tracking and energy resolution. Through private communication in August 2014 with Dr. Andre Schöning, the contact person at Mu3e, we have been told that the mass resolution is $\sigma_m/m \approx 0.004$. This holds best for the heavier mediators in the mass range of $10 - 100$ MeV. Lighter invariant mass pairs, ~ 1 MeV, are harder to distinguish, as the decay angle is small and the resolution is limited by multiple scattering. For now, we simply use the mass resolution at 10 MeV, for the low mass limit of our generated events, but one must keep in mind that below 10 MeV the results will likely be overly optimistic.

With this mass resolution in mind, we bin each of the invariant mass spectra. After scaling up the total number of events to 10^{15} (5.5×10^{16}) for Mu3e phase I (phase II), scaling the signal events by the branching ratio of the signal, and scaling the background events by the SM branching ratio, we are ready to use the spectrum. We also rescaled by a factor of 137/127.9 for the running of the α coupling, as MadGraph by default uses α evaluated at the mass of the Z. The scaling by the branching ratios ensures that we have the correct number of expected total signal events, and background events. An example spectrum with both signal and background is shown

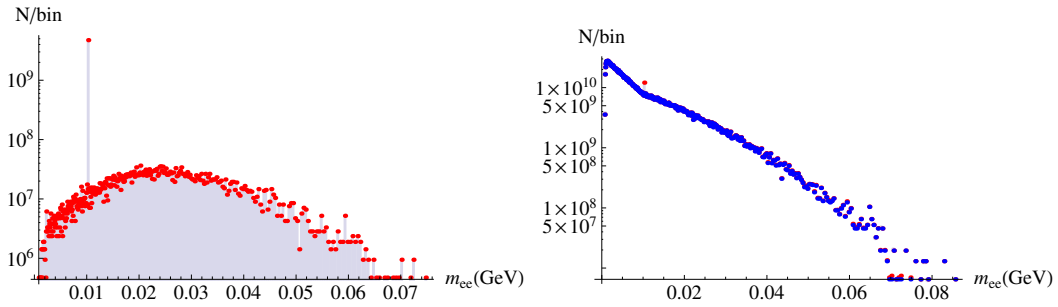

Figure 5.3: Sample invariant mass spectrum from events generated by MadGraph. Events in red correspond to signal events, and events in blue correspond to background events. **Left**: The signal spectrum. Note the narrow resonance corresponding to the production of the scalar mediator. The smooth variation below the resonance is attributed to the reconstruction of the e^+e^- pair using the positron whose parent is not the ϕ. To enhance the peak visibility, $g_{\phi\mu} = 0.01$ is used. **Right**: The signal and background spectrum. The resonance is slightly visible above the background, centered at the mass used during generation. Elsewhere on the spectrum the signal is not visible.

in Fig. 5.3.

Once we have a spectrum, it is easy to find the limiting coupling according to our prescription in section 4.3 and equation 5.1. Instead of analyzing the total number of signal and background events, we can do better by using the spectrum and focusing on the region where the resonance occurs. This reduces the background within the bin to a much more reasonable level for sensitivity, and also keeps all of the signal, since we are dealing with a very narrow width. To implement this, we ask for the bin with maximum signal, look up the corresponding background level, and compute $g_{\phi\mu}^{\text{limit}}$ to 3σ. The resulting sensitivity limits are shown in Fig. 5.4.

We also make use of an existing study of the dark photon at the Mu3e experiment to obtain limits in a similar fashion. Echenard et. al. have done this using a similar method, using MadGraph to generate events and then inserting a proper detector simulation [49]. Their limits extend for a dark photon mass range of $10 - 80$ MeV, as the dark photon is mostly ruled out already below 10 MeV. This removes any need for us to do background simulation for this case. In order to translate their limits from the dark photon case to the scalar case, we must do a simple simulation of the dark photon signal ourselves. Using the dark photon model developed earlier for MadGraph, we perform the same generation of events as outlined for the scalar. We set the dark photon kinetic mixing to $\epsilon = 0.1$, and generate signal events over

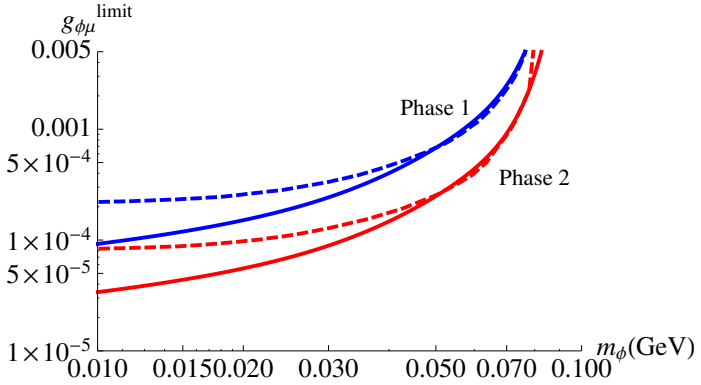

Figure 5.4: Sensitivity limits on the scalar coupling to muon using μ^+ decay at Mu3e. Results using our background simulation are shown as solid lines, while results translated using Echenard et. al. are shown as dashed lines [49]. In blue are the phase I limits, and in red are the phase II limits. The dark photon results should have a more robust background and detector simulation than our simple treatment. Our background simulation allows for sensitivity limits lower than 10 MeV, however the resolution of the invariant mass of the e^+e^- pair is relatively unknown here, so we limit ourselves to $m_\phi > 10$ MeV.

the same 200 mass points. Equating the number of signal events between the two models for the given limiting ϵ and an unknown limiting $g_{\phi\mu}$, lets us translate the limits, since the number of events detected for sensitivity must be the same. Doing this, we find the following result:

$$g_{\phi\mu}^{\text{limit}} = g_{\phi\mu}^{\text{test}} \frac{\epsilon^{\text{limit}}}{\epsilon^{\text{test}}} \sqrt{\frac{\text{BR}(\mu^+ \to e^+ \bar{\nu}_\mu \nu_e A')}{\text{BR}(\mu^+ \to e^+ \bar{\nu}_\mu \nu_e \phi)}} \tag{5.7}$$

In this expression, the branching ratios and ϵ^{limit} are all a function of mass, with the branching ratios coming from our simulation and the limiting kinetic mixing from [49]. The resulting limits can be seen in Fig. 5.4.

Comparing the results of the two methods, the plateauing behaviour towards low mass mediators is more likely correct than our treatment of a fixed mass resolution below 10 MeV. As expected, our results are more optimistic. This is likely because we are not taking into account detector efficiencies, which will degrade the signal sensitivity towards the lower masses. Nonetheless, the agreement everywhere towards the higher mass end suggests that our simulation is robust enough while also being relatively simple in concept.

5.2 Sensitivity Reach of NA48/2 and NA62 from Charged Kaon Decays

In contrast to the previous section on muon decay, the calculations of kaon decay are relatively easy to handle and can be done analytically. We still make use of FeynCalc in order to compute the traces and Mathematica to compute the final-state integration, although it is not necessary under certain approximations and is computable by hand. While NA48/2 and NA62 will not reach a number of kaon decays comparable to the muon decays, we still have 2.0×10^{11} K^+ decays at NA48/2 and an expected 9.0×10^{12} K^+ decays at NA62. These numbers are large enough to put strong bounds on the scalar, but likely not as strong as those from Mu3e. NA48/2 and NA62 will have many kaons decaying with a forward momentum of 75 GeV $\pm 1\%$ while in the fiducial volume, so we must take care that the forward detector will be able to collect any decay products suggested. The signature we are interested in is similar to the muon decay as well: a resonance in the invariant mass spectrum of decay products for the leptonic process $K^+ \to \mu^+\nu_\mu\ell^+\ell^-$, with $\ell = e, \mu$, depending on the available energy. For the signal, the scalar will radiate off of the anti-muon. This channel will dominate over emission from a positron, $K^+ \to e^+\nu_e\phi$, due to the larger coupling to muons. Furthermore, the background is more complicated and requires special treatment, which we will talk about now.

5.2.1 Backgrounds

We must first break down the mass regions that we are interested in. For $m_\phi < m_{\pi^0}$, the background is dominated by the Dalitz decay

$$K^+ \to \mu^+ + \nu_\mu + \pi^0,\ \pi^0 \to e^+ + e^- + \gamma. \tag{5.8}$$

This will appear as a background if the photon is not detected. The production of the $\mu^+\nu_\mu$ can come also from a π^+ decay which comes with a branching ratio ~ 1, produced via $K^+ \to \pi^+\pi^0$. This proves to be a very strong background source for the low mass part of the spectrum. Since we expect our signal to be very narrow, as the width of the scalar is very small, we can examine the differential decay rate in the e^+e^- invariant mass, which is well known. The number of background events is given in equations 5.9. The expression for $\Gamma(\pi^0_D)$ is given by [68].

$$B(m_{ee}) = N_{K^+}\ \mathrm{BR}(K^+ \to \mu^+\nu_\mu\pi^0)\ \frac{d\Gamma(\pi^0_D)}{dm_{ee}}\frac{\sigma_{m_{ee}}}{\Gamma(\pi^0_{2\gamma})}\mathrm{BR}(\pi^0_{2\gamma})\ \Pr(\text{lose }\gamma) \quad (5.9)$$

$$\frac{1}{\Gamma(\pi^0_{2\gamma})}\frac{d\Gamma(\pi^0_D)}{dx} = \frac{2\alpha}{3\pi}\frac{(1-x)^3}{x}(1+\frac{r^2}{2x})\sqrt{1-\frac{r^2}{x}}\,|F(x)|^2 \quad (5.10)$$

$$x = \left(\frac{m_{ee}}{m_{\pi^0}}\right)^2 \quad (5.11)$$

$$r^2 = 4m_e^2/m_{\pi^0}^2 \approx 5.73\times10^{-5} \quad (5.12)$$

$$F(x) = 1 + ax \approx 1 + 0.03x \quad (5.13)$$

We will now carefully go over these equations as presented. First, for the Dalitz decay to be considered a source of background, we must not detect the photon. We take this to have probability $\Pr(\text{lose }\gamma) = 10^{-3}$. A typical inefficiency for high energy photons in NA62 is a few times 10^{-4} [39], which will be slightly worse for any lower energy photons, so we take a slightly pessimistic view and use 10^{-3}. Secondly, the total number of Dalitz decays in one bin of m_{ee} must depend on the width of the bin, $\sigma_{m_{ee}}$, and we normalize to the total decay width of the positively charged kaon. Also, the number of background events comes directly from the K^+ decays, where we take $\mathrm{BR}(K^+ \to \mu^+\nu_\mu\pi^0) = 0.03352 + 0.2067 = 0.24022$ to be the sum of the semileptonic and hadronic modes [37]. Finally, the function $F(x)$ is the π^0 form factor, which usually appears when dealing with mesons and is simply approximated as a linear expansion with a small slope that is measured. Later, we will set $m_{ee} = m_\phi$ since all of our signal will fall into the one bin.

Outside of this range, the other irreducible backgrounds that take over are split into two ranges. For 150 MeV $< m_{ee} < 2m_\mu$, the dominant decay is $K^+ \to \mu^+\nu_\mu e^+e^-$, which has a measured branching ratio of 7.06×10^{-8}. Below 150 MeV, this background is hard to measure due to cuts made that keep the lepton pair mass above the pion threshold. Currently it is not known if NA62 will be able to study lepton pairs with a mass below the pion mass. Since we do not know the distribution of these events in m_{ee}, for this study we take the simplistic assumption that they are distributed up to the kinematic limit of $m_K - m_\mu$ according to the phase space factor. We reweight the background by this factor using the distribution of background events shown in Fig. 5.3, stretched up to the kinematic limit relevant for the kaon decay, and enforce that the normalization corresponds to the branching ratio above $m_{ee} >$

150 MeV. This background distribution is used because the e^+e^- pairs in $\mu^+ \to e^+\nu_e\bar{\nu_\mu}e^+e^-$ come mostly from final state radiation, similar to the pairs produced in $K^+ \to \mu^+\nu_\mu e^+e^-$, so the backgrounds should be similar. This can be improved by using Monte Carlo techniques to generate this background distribution as well, or by calculating the distribution directly. The result of using this distribution compared to the true one likely yields over-sensitivity projections at lower masses and under-sensitivity projections at higher masses.

When the muon decay channel turns on for the scalar, we must then look at the background due to $K^+ \to \mu^+\nu_\mu\mu^+\mu^-$. Currently this is not observed and there are only limits on the branching ration of $< 4.1\times10^{-7}$ [37]. In the absence of background, the simplest thing that we can do is set a constant number of events to indicate the presence of a signal. Since this decay is currently not observed, we set the sensitivity to be where there are 5 signal events in this region.

For the mass resolution, one consideration is to simply use the energy resolution. This is not ideal however, as the mass resolution is typically better than the energy resolution since it is also possible to track the particles momenta. We utilize the same mass resolution given in [48], as extracted from Monte Carlo, where they find $\sigma_{m_{ee}} = 0.067 \text{ MeV} + 0.0105 m_{ee}$.

5.2.2 Signal

Here we will actually compute the decay width of the kaon contribution from our process by hand. The signal we are interested in is

$$K^+ \to \mu^+ + \nu_\mu + \phi,\ \phi \to \ell^+ + \ell^-. \tag{5.14}$$

Both channels ($\ell = e, \mu$) can be treated at the same time, as we treat ϕ as being on-shell and following the decay chain. The Feynman diagram for the process we are interested in is shown in Fig. 5.5.

We can compute this by making use of the Dalitz plot, where one integrates over the squares of the invariant masses of the final state pairs. This means we will integrate over any pair of $m^2_{\mu\nu}$, $m^2_{\mu\phi}$, and $m^2_{\phi\nu}$, instead of over the energies of the outgoing particles. The reason for doing this is that the matrix element is usually expressed in a simpler fashion using these variables and the boundaries are easier to define. It also reads in a more explicitly covariant manner. The pair of variables we choose to integrate over are $m^2_{\mu\nu}$ and $m^2_{\mu\phi}$. $m^2_{\mu\nu}$ is chosen because it only appears

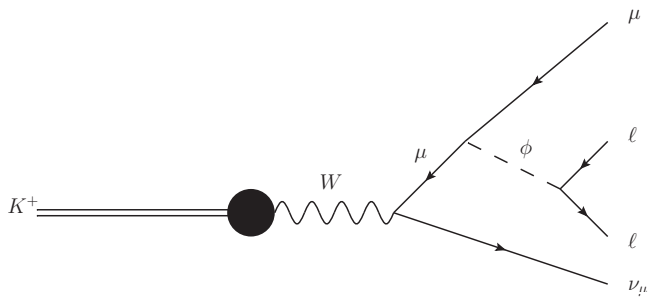

Figure 5.5: Feynman diagram for charged kaon decay through the scalar. The scalar decays to either an e^+e^- pair, or a $\mu^+\mu^-$ pair, depending on the mass available to the scalar, which is taken to be on-shell. The blob represents them form factor for the kaon.

in the numerator for our process as a simple polynomial when used in conjunction with the other variable, $m^2_{\mu\phi}$. $m^2_{\mu\phi}$ is chosen because the propagator for the internal muon appears as $\left(m^2_{\mu\phi} - m^2_{\mu}\right)^{-1}$ and is naturally expressed in this variable. In the *Kinematics* section of [37], the Dalitz plot is specified in these variables as a density of the squared matrix element. An example plot is shown for $m_\phi = 100$ MeV in Fig. 5.6.

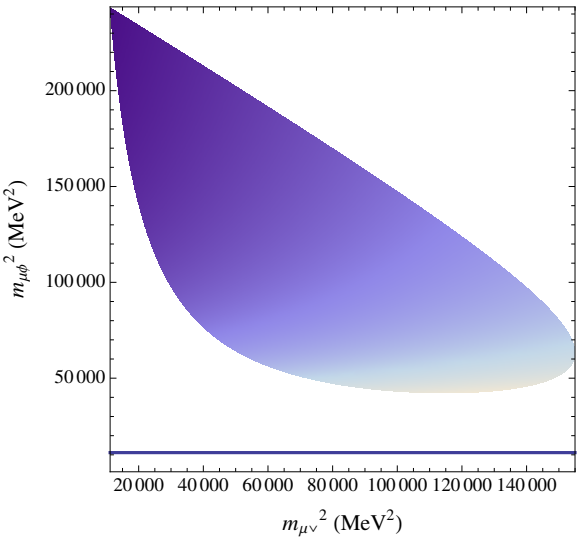

Figure 5.6: Dalitz plot for charged kaon decay. The horizontal line corresponds to the resonant condition $m^2_{\mu\phi} = m^2_{\mu}$. As the scalar gets lighter, the density gets higher, showing that the density of the amplitude increases as one approaches the resonant condition. Here it is not possible to hit the resonance, but as m_ϕ gets very small, we get close to it.

The allowable region is precisely defined below.

$$(m^2_{\mu\nu})_{\max/\min} = m^2_\mu + \frac{1}{2m^2_{\mu\phi}}\left(\left(m^2_K - m^2_{\mu\phi}\right)\left(m^2_{\mu\phi} - m^2_\phi + m^2_\mu\right) \pm \sqrt{\lambda\left(m^2_{\mu\phi}, m^2_K, 0\right)\lambda\left(m^2_{\mu\phi}, m^2_\phi, m^2_\mu\right)}\right) \tag{5.15}$$

λ is defined as $\lambda(x,y,z) = x^2+y^2+z^2-2xy-2xz-2yz$. After doing this integration, it is then straightforward to integrate over all allowable values of $m^2_{\mu\phi} \in [(m_\mu + m_\phi)^2, m^2_K]$, to obtain the total rate. Carrying out this process yields the width as a function of mass m_ϕ, and the resulting branching ratio can be seen in Fig. 5.7.

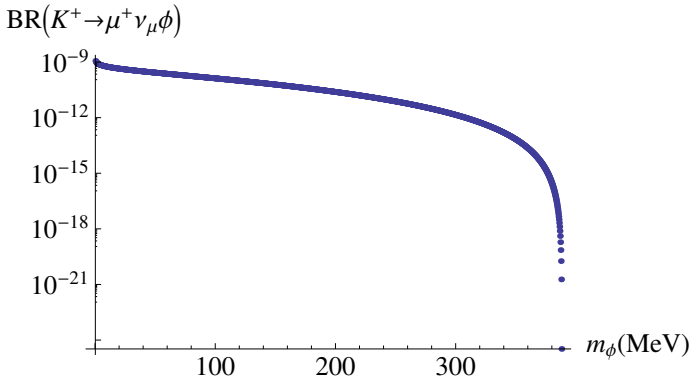

Figure 5.7: Branching ratio of $K^+ \to \mu^+\nu_\mu\phi$. The coupling is taken to be $g_{\phi\mu} = 10^{-4}$. There is an increased rate at extremely low energies and a quick downturn near $m_K - m_\mu$, where the phase space closes rapidly.

Finally, we can use the signal branching ratio combined with our backgrounds to set a limit on the coupling. The number of signal events we see is

$$S = N_{K^+}\ \mathrm{BR}(K^+ \to \mu^+\nu_\mu)\frac{\Gamma(K^+ \to \mu^+\nu_\mu\phi)}{\Gamma(K^+ \to \mu^+\nu_\mu)}\ \mathrm{BR}(\phi \to \ell^+\ell^-), \tag{5.16}$$

where ℓ is either a muon or an electron. We have chosen to normalize to the two body decay rate to remove any dependence on the kaon form factor. For the two body decay rate, it is easy to find the following expression:

$$\Gamma(K^+ \to \mu^+\nu_\mu) = \frac{1}{8\pi m^3_K} f^2_K\,|V_{us}|^2\,G^2_F m^2_\mu\left(m^2_K - m^2_\mu\right)^2 \tag{5.17}$$

In the limit of $m_\phi \ll m_\mu$, we find the following behaviour:

$$\frac{\Gamma(K^+ \to \mu^+ \nu_\mu \phi)}{\Gamma(K^+ \to \mu^+ \nu_\mu)} = \frac{1}{4\pi^2} \ln\left(\frac{m_K^2 - m_\mu^2}{2 m_\phi m_\mu}\right) \tag{5.18}$$

For $m_\phi = 100$ MeV, the branching ratio is

$$\mathrm{BR}(K^+ \to \mu^+ \nu_\mu \phi) = 1.32 \times 10^{-10} \left(\frac{g_{\phi\mu}}{10^{-4}}\right)^2 . \tag{5.19}$$

Combining the number of signal events with the number of background events in each background region, we find the limits that are shown in Fig. 5.8. We also assume an overall signal efficiency of 0.5. Since the kaons are boosted, a rough approximation on the maximum angle from the beam that any decay products can have is $\theta_{\max} \approx \frac{m_K/2}{p_K} \approx 3$mrad, which stays within the calorimeter's 8.5mrad coverage, so most of the decay products produced should pass through the detector. To be safe though, we choose the efficiency above. Above the pion mass, the sensitivity starts to increase as the Dalitz background disappears. The Dalitz decay quickly vanishes near the pion mass, however the other relevant backgrounds in this region are unknown, with the SM process $K^+ \to \mu^+ \nu_\mu e^+ e^-$ only being measured for $m_{ee} > 150$ MeV, as discussed earlier.

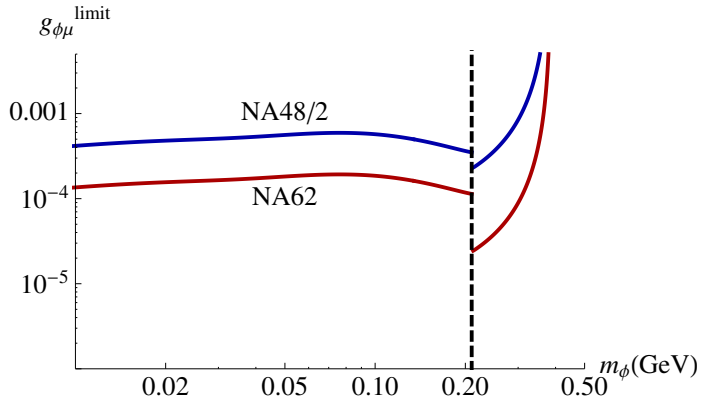

Figure 5.8: Sensitivity limits on scalar coupling to muon from charged kaon decays. Blue lines correspond to NA48/2 and red to NA62. The dashed line indicated the dimuon threshold, where our definition of the signal and background changes. Below the pion mass, the Dalitz background and the $K^+ \to \mu^+ \nu_\mu e^+ e^-$ background are both present. The Dalitz background is not present above the pion mass, where the irreducible backgrounds to either $\mu^+ \nu_\mu e^+ e^-$ for $m_{ee} < 2m_\mu$, or $\mu^+ \nu_\mu \mu^+ \mu^-$ for $m_{ee} > 2m_\mu$, take over.

5.3 Sensitivity Reach of B-factories from e^+e^- Annihilation

For e^+e^- collisions, we make use of MadGraph again to handle our signal and background estimates. Most of what was said about the generation of events for the muon decay case holds here.

The total integrated luminosities at Belle is taken to be 1040.86 fb^{-1}, with BaBar at half of this, and Belle2 to be expected to have around 100 times this. All of the BaBar and Belle data is already taken and stored. This means that an analysis performed by the experiments of the data already taken could cover a large area of the parameter space. The large integrated luminosities used will allow very competitive sensitivity limits compared to the other experiments discussed. Since the centre-of-mass energy reaches 10.58 GeV, we can access the τ leptons here which, in our model have a very strong coupling to the scalar due to their large mass of 1.777 GeV. We are interested in the mediator mass regions that are above and below the threshold for the scalar to decay to muons. Below this, it can only decay to an e^+e^- pair, so the overall process for $m_\phi < 2m_\mu$ is

$$e^+ + e^- \to \tau^+ + \tau^- + e^+ + e^-, \tag{5.20}$$

while above this threshold we decay almost exclusively to muons,

$$e^+ + e^- \to \tau^+ + \tau^- + \mu^+ + \mu^-. \tag{5.21}$$

5.3.1 Backgrounds

Here we simply write down the irreducible SM background process and let MadGraph run. We generate $10,000$ background events for each of the two final states. A sample Feynman diagram is shown in Fig. 5.9.

5.3.2 Signal

Again, we simply define our process and let MadGraph run, akin to the muon decay generation. $10,000$ events are generated at each of the 20 mass points from $2m_e$ up to $2m_\mu$, and again from $2m_\mu$ up to $2m_\tau$. However, we do not go above $2m_\tau$ for simplicity, as this will open the 4τ channel, where the signature does not have the advantage of

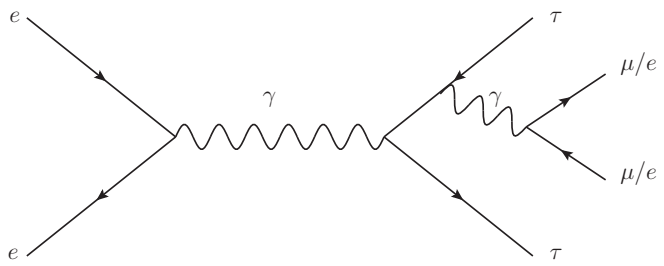

Figure 5.9: One Feynman diagram for the background process $e^+e^- \to \tau^+\tau^-\ell^+\ell^-$.

being a spectrally peaked signal. We enforce that the generation of the scalar is once again on-shell, so our process is really the decay chain below:

$$e^+ + e^- \to \tau^+ + \tau^- + \phi,\ \phi \to \ell^+ + \ell^- \tag{5.22}$$

A sample Feynman diagram for the signal is shown in Fig. 5.10.

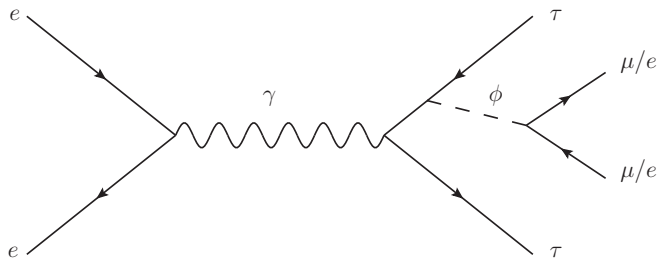

Figure 5.10: One Feynman diagram for the signal process $e^+e^- \to \tau^+\tau^-\ell^+\ell^-$. The scalar must live on-shell before decaying promptly to a pair of leptons.

As with the other signals we have examined with an e^+e^- pair in the final state, we must take into account the reduced number of signal events due to the branching ratio to the process $\phi \to \gamma\gamma$. This is only important for masses of the scalar just below the dimuon production threshold.

For our signal, since this is now a collision scenario and not a decay, we must weight our total number of events by the cross section determined by MadGraph. The bin width we have chosen is also just the energy resolution of the detector listed in the technical design report for Belle2 [44] as

$$\frac{\sigma_E}{E} = \sqrt{\left(\frac{0.066\%}{E}\right)^2 + \left(\frac{0.81\%}{E^{1/4}}\right)^2 + (1.34\%)^2}, \tag{5.23}$$

with E being measured in GeV.

One of the more interesting aspects of this signal is that we do not need to fully reconstruct both outgoing τ particles. It is sufficient that we have one of them decay leptonically, $\tau^- \to \ell^- \bar{\nu}_\ell \nu_\tau$ (or the conjugate decay), which comes with a total branching fraction BR $= 0.1742 + 0.1783 = 0.3524$ [37]. We allow all decay modes for the other τ. Thus, our signal really is three charged leptons in the final state, and either hadrons, leptons, or missing energy, with two same-flavour oppositely-charged leptons reconstructing to the same invariant mass. It should be noted that while we currently do not do this, there are known efficiencies for $\tau \to 4\ell$ that we can use to account for this correctly. The cross section found at $m_\phi = 10$ MeV relative to the production of a pair of taus is

$$\frac{\sigma\left(e^+e^- \to \tau^+\tau^-\phi, m_\phi = 10 \text{ MeV}\right)}{\sigma\left(e^+e^- \to \tau^+\tau^-\right)} = 2.9 \times 10^{-9} \left(\frac{g_{\phi\tau}}{10^{-4}}\right)^2 . \tag{5.24}$$

Additionally, we only introduce a total efficiency of 0.5 to be safe, as there should be some acceptance loss when trying to distinguish the lepton produced from the tau decay and one of the leptons in the pair. An acceptance loss could be accepted here because these should be well-separated in angular variables. We also need to correct for the appropriate scalar coupling, as the one of importance in this scenario is the coupling to the tau, so any sensitivity limits set must be scaled down to that of the muon. Finally, we limit our final results to have $m_\phi > 20$ MeV, as a similar search for the dark photon at BaBar did not go lower than this [69].

The full sensitivity limits are presented in Fig. 5.11. A simple analysis at BaBar and Belle could already exclude a large portion of the parameter space.

It is also possible to look for the signal

$$e^+ + e^- \to \mu^+ + \mu^- + \phi,\ \phi \to \mu^+ + \mu^- \ . \tag{5.25}$$

The benefit of searching for such a signal is that we could reach masses of the scalar up to 10 GeV. Unfortunately, this also comes with the drawback of a reduced number of signal events compared to the tau channel, since $g_{\phi\mu}/g_{\phi\tau} = m_\mu/m_\tau$. We will not examine the properties of this signal in this thesis, but it is possible to do with the tools developed so far.

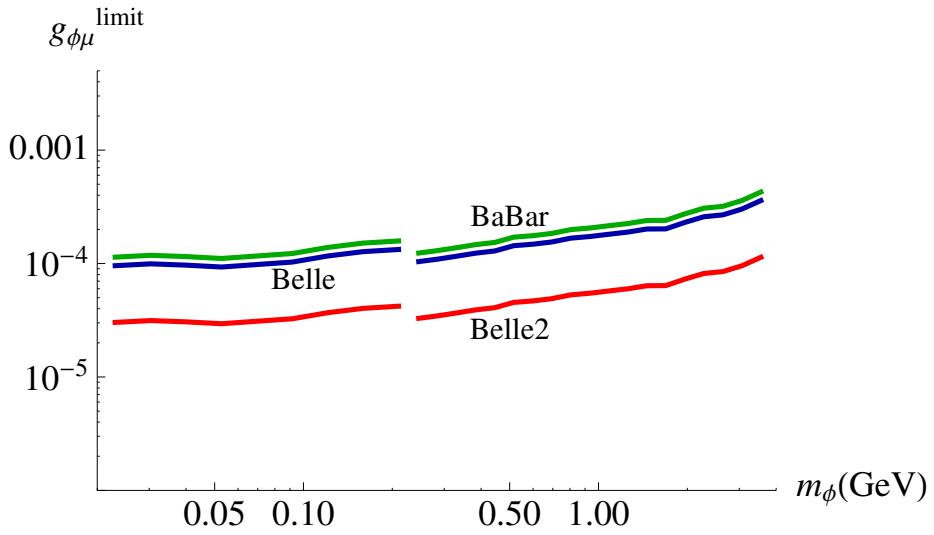

Figure 5.11: Scalar limits from e^+e^- collisions at B-factories. Green, blue, and red lines represent BaBar, Belle, and Belle2 respectively. The region where the muon channel turns on can be seen, where we remove a small portion of the parameter space due to poor background simulation in the vicinity of the very soft dimuon pair. At this point the $\phi \to \gamma\gamma$ decay is strongest also, and reduces the sensitivity right before the dimuon channel opens.

Chapter 6

Conclusion

Our goal for this thesis was to find the sensitivity of three classes of experiments to a new MeV scale force and compare the results with the range of couplings suggested with the $(g-2)_\mu$ and anomalous r_p results. The most sensitive projections are shown in Fig. 6.1.

Utilizing the Monte Carlo generator MadGraph, we were able to phenomenologically explore the new scalar particle. Restricting this particle to decay only to SM particles, in particular, pairs of leptons, allows one to put stringent bounds on the coupling, down to the level of 10^{-5} for the coupling to the muon. Unlike the case of the dark photon that is thoroughly studied, much of the parameter space for the scalar remains unexplored. A region of the currently allowed parameter space could serve as an explanation for the proton radius problem and the $(g-2)_\mu$ discrepancy. Upcoming experiments offer a chance to test physics at the intensity frontier where many decays and collisions take place, allowing restrictions on branching ratios of SM physics to be placed down to the level of 10^{-16} in coming years. The data collected from these experiments will be used to test this model and many other low mass theories. The sensitivity limits placed were on the experiments Mu3e, NA48/2, NA62, BaBar, Belle, and Belle2, across a large mass range from $2m_e$ up to $2m_\tau$.

There is also a large amount of future work that can be performed by the experimental collaborations to obtain a more accurate representation of the upper limits at these experiments. First, a more robust treatment of the detectors would be a sensible way to proceed. Most experiments likely have a Geant4 model that would be useful in these scenarios. At the very least, performing Monte Carlo to find the signal efficiencies and mass resolution with these models would bear the most fruit, as these are hard to estimate without a robust Monte Carlo code. Currently we use

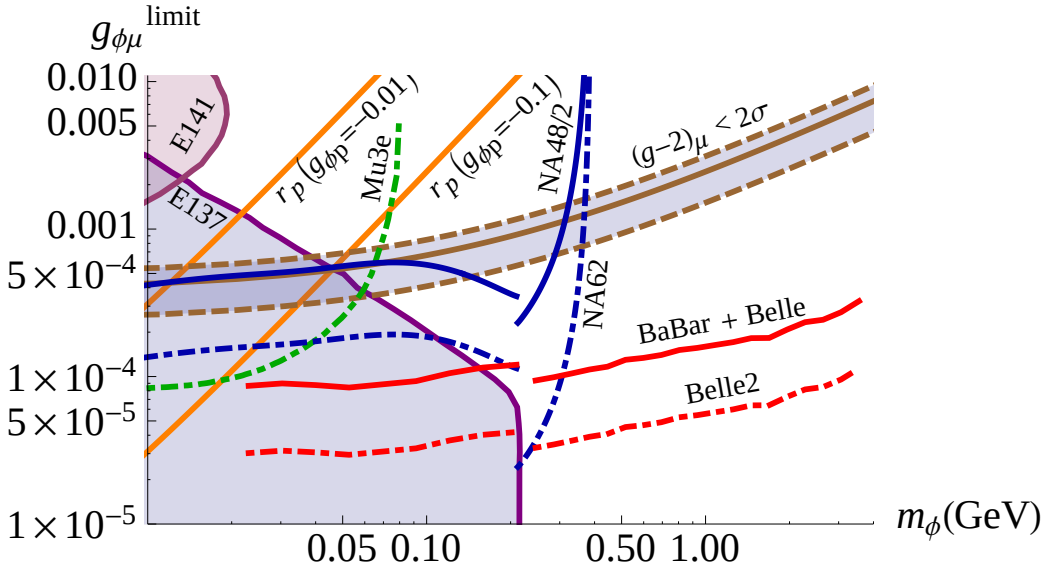

Figure 6.1: Collection of the most promising sensitivity projections found in this work. Green shows the limits of phase II of Mu3e, blue shows the NA48/2 and NA62 experiments, and red shows the combined Belle and BaBar experiments, and Belle2 experiment. In purple are the constraints from the E137 and E141 beam dump experiments, as found in [30, 31]. Dot-dashed lines correspond to experiments not yet run, while solid lines correspond to data already taken. The band indicated by the brown and brown-dashed curves is the region where the 2σ anomaly of $(g-2)_\mu$ could be solved. In orange are contours that solve the proton radius problem for fixed coupling to the proton.

the condition that $S = 3\sqrt{B}$ for sensitivity in most cases, and then examine a signal bin; this could be improved with a proper likelihood fit or by utilizing a Feldman-Cousins technique. However, doing this has diminishing returns since we are merely projecting expected limits and not actively searching for any. In the B-factory cases, it is also possible to go beyond $2m_\tau$ if we consider a signal with muons in the final state instead of taus. Variants on the model can also be discussed. We may attempt to put a pseudo-scalar into the model, or examine the vector or axial-vector cases, or even simply play with the coupling strength being proportional to the lepton masses. Finally, more experiments are being pursued that may be able to shine light on portions of the parameter space. Fermilab will soon have a new measurement of $(g-2)_\mu$, and the proton charge radius with muons will be studied by scattering muons off of protons at MUSE. Other experiments such as Mu2e [70] or COMET [71] could similarly play an important role when examining lepton flavour violation in the charged lepton sector. We conclude by noting that there is the possibility for this model to be

tested rigorously and the parameter space explored over the next few years by many experiments, some of which were discussed in detail in this thesis.

Appendix A

Model Generation Files

We provide the relevant files for generating a usable FeynRules model for the models used in this thesis.

A.1 Scalar Model

A.1.1 `scalar.fr` Field Definition

This file defines the scalar field and its parameters. Note that it does not say anything about the width, which will be automatically computed for all available $1 \to 2$ processes when generating events. It also does not contain any information on the allowed interactions, which come in the model file.

```
M$ModelName = "scalar";

M$Information = { Authors      -> { "N. Lange" },
                  Version      -> "1.3",
                  Date         -> "May 27, 2015",
                  Institutions -> { "University of Victoria" },
                  Emails       -> { "nlange@uvic.ca" }
                };

M$ClassesDescription = {
    S[100] == {
        ClassName        -> phi,
        SelfConjugate    -> True,
        Mass             -> { Mphi, 1 },
        Width            -> { Wphi, 1 },
        PropagatorLabel  -> "phi",
        PropagatorType   -> D,
        PropagatorArrow  -> None,
        ParticleName     -> "phi",
```

```
        FullName          -> "Dark Scalar"
    }
};

M$Parameters = {
    gst == { ParameterType    -> External,
             Value            -> 1,
             InteractionOrder -> { NP, 1 }
    },

    gsm == { ParameterType    -> Internal,
             Value            -> gst*MMU/MTA,
             InteractionOrder -> { NP, 1 }
    },

    gse == { ParameterType    -> Internal,
             Value            -> gst*Me/MTA,
             InteractionOrder -> { NP, 1 }
    }
};
```

A.1.2 `scalar.m` Lagrangian and Feynman Rules

This file defines the Lagrangian to be used, including both the freely propagating component and the interaction component. FeynRules is invoked to produce a computationally usable model.

```
(* ::Package:: *)

<< "FeynRules`"

LoadModel["SM.fr", "scalar.fr"];

\[ScriptCapitalL]new = (1/2)*del[phi, \[Mu]]*del[phi, \[Mu]] - (Mphi^2/2)*phi^2 +
   gsm*mubar . mu*phi + gse*ebar . e*phi + gst*tabar . ta*phi

vertices = FeynmanRules[\[ScriptCapitalL]new]
decays = ComputeWidths[vertices]

UpdateWidths[decays]

(* Skip checking the Hermiticity since it is slow; this should be re-enabled when the
    ↪ model changes *)
(* CheckHermiticity[LSM + \[ScriptCapitalL]new] *)

WriteUFO[LSM + \[ScriptCapitalL]new]
```

A.2 Dark Photon Model

The same comments regarding the scalar model hold here also.

A.2.1 `darkphoton.fr` Field Definition

Unlike the scalar model, we must define the $U(1)'$ gauge group here.

```
M$ModelName = "darkphoton";

M$Information = { Authors      -> { "N. Lange" },
                  Version      -> "1.0",
                  Date         -> "December 4, 2014",
                  Institutions -> { "University of Victoria" },
                  Emails       -> { "nlange@uvic.ca" }
                };

M$GaugeGroups = {
    U1D == {
        Abelian          -> True,
        CouplingConstant -> eps,
        GaugeBoson       -> Ad,
        Charge           -> Q
    }
};

M$ClassesDescription = {
    V[100] == {
        ClassName        -> Ad,
        SelfConjugate    -> True,
        Mass             -> { Mad, 1 },
        Width            -> { Wad, 1 },
        PropagatorLabel  -> "ad",
        PropagatorType   -> W,
        PropagatorArrow  -> None,
        ParticleName     -> "ad",
        FullName         -> "Dark Photon"
    }
};

M$Parameters = {
    eps == { ParameterType    -> External,
             Value            -> 1,
             InteractionOrder -> { NP, 1 }
    }
};
```

A.2.2 `darkphoton.m` Lagrangian and Feynman Rules

Note that FeynRules has a function `FS`, which is allows one to use the field strength tensor when formulating a Lagrangian.

```
(* ::Package:: *)

<< "FeynRules`"

LoadModel["SM.fr", "darkphoton.fr"];

\[ScriptCapitalL]new = (-(1/4))*FS[Ad, \[Kappa], \[Tau]]*FS[Ad, \[Kappa], \[Tau]] +
    ↪ (1/2)*Mad^2*Ad[\[Kappa]]*Ad[\[Kappa]] +
   eps*ee*ebar . Ga[\[Kappa]] . Ad[\[Kappa]] . e + eps*ee*mubar . Ga[\[Kappa]] . Ad
       ↪ [\[Kappa]] . mu

\[ScriptCapitalL]new = ExpandIndices[\[ScriptCapitalL]new];

vertices = FeynmanRules[\[ScriptCapitalL]new]
decays = ComputeWidths[vertices]

UpdateWidths[decays]

(* Skip checking the Hermiticity since it is slow; this should be re-enabled when the
    ↪ model changes *)
(* CheckHermiticity[LSM + \[ScriptCapitalL]new] *)

WriteUFO[LSM + \[ScriptCapitalL]new]
```

Appendix B

MadGraph Generated Feynman Diagrams

For any processes that are sampled using MadGraph, the resulting diagrams used are all displayed here.

B.1 Muon Decay

These are all the Feynman diagrams when doing the muon decay calculation. Here we sample the background, the scalar signal, and also the dark photon signal.

B.1.1 Standard Model Background

All background diagrams sampled are shown in Fig. B.1. Note that some of these diagrams have multiple W propagators, and will be heavily suppressed by an extra factor of G_F^2 compared to the diagrams with a single W. There are also diagrams which were omitted carrying a Z instead of a photon, and of course the Higgs diagrams are excluded without any loss of accuracy.

B.1.2 Scalar Signal

All signal diagrams sampled for the scalar are shown in Fig. B.2. In these diagrams, keep in mind that the scalar is required to be *on-shell*. It is also assumed that the scalar has a narrow width and will decay promptly. This restricts the number of

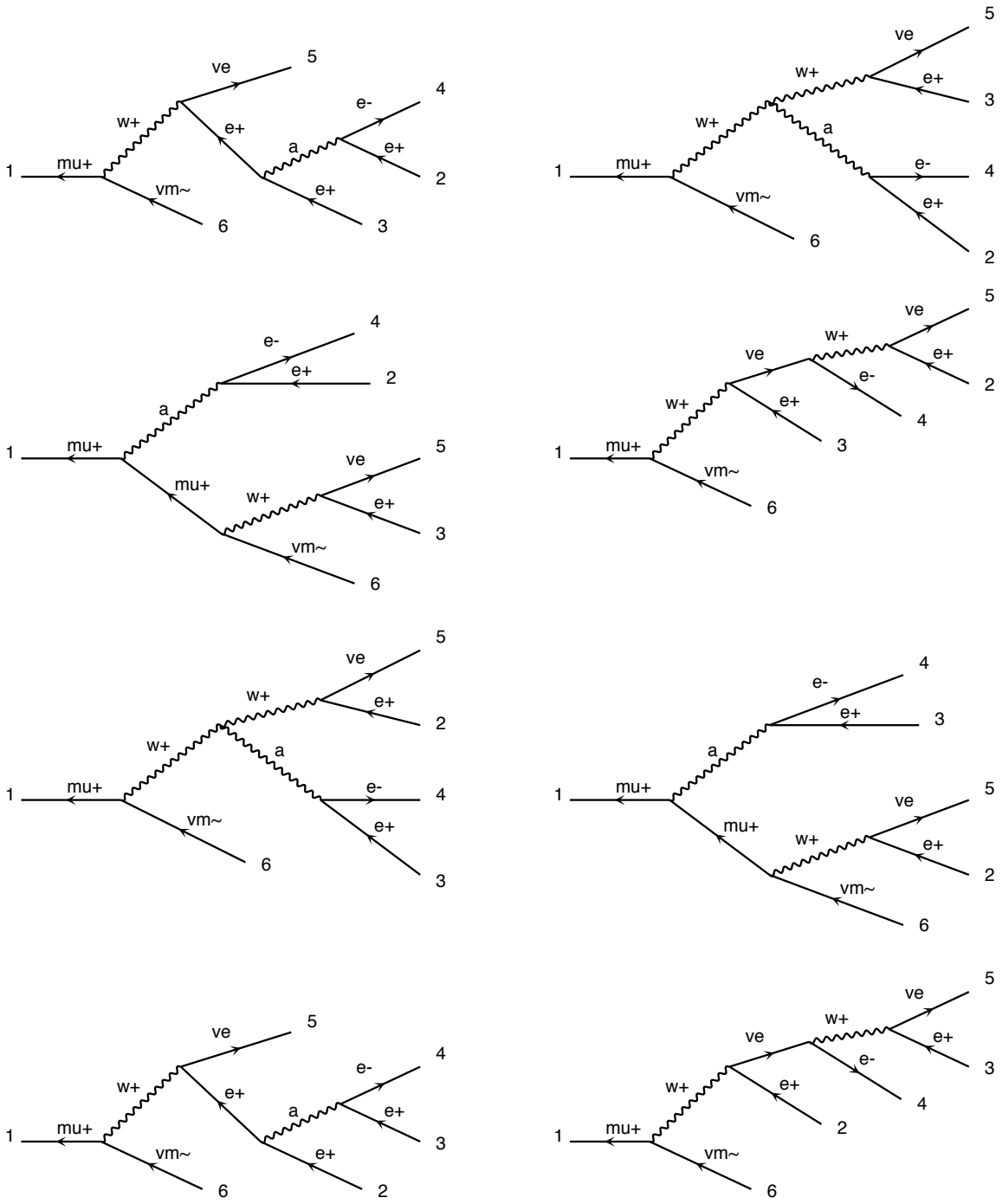

Figure B.1: SM background contribution to muon decay with an extra e^+e^- pair in the final state. Nothing is required to be on-shell here by default.

diagrams and also forces MadGraph to compute the decay as a decay chain instead of a single decay.

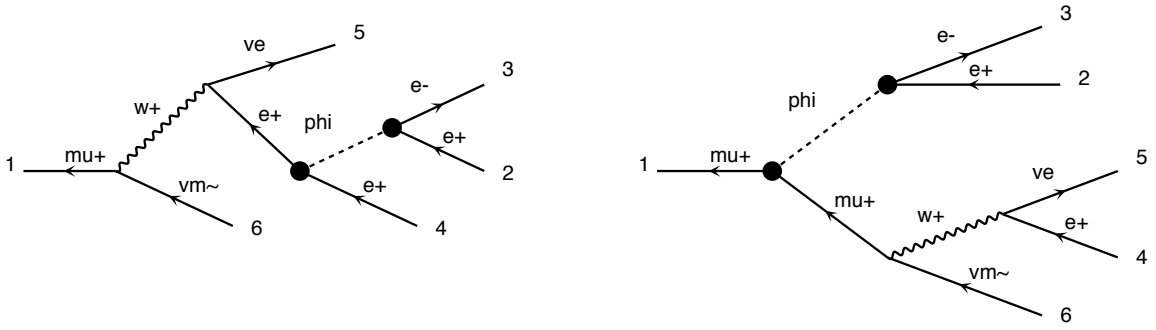

Figure B.2: Signal contribution to muon decay from the scalar field. The scalar is taken to be on-shell where it decays to an e^+e^- pair.

B.1.3 Dark Photon Signal

All signal diagrams sampled for the dark photon are shown in Fig. B.3. Again, the dark photon here is required to be produced *on-shell*. The same comment regarding the width of the dark photon can be said here.

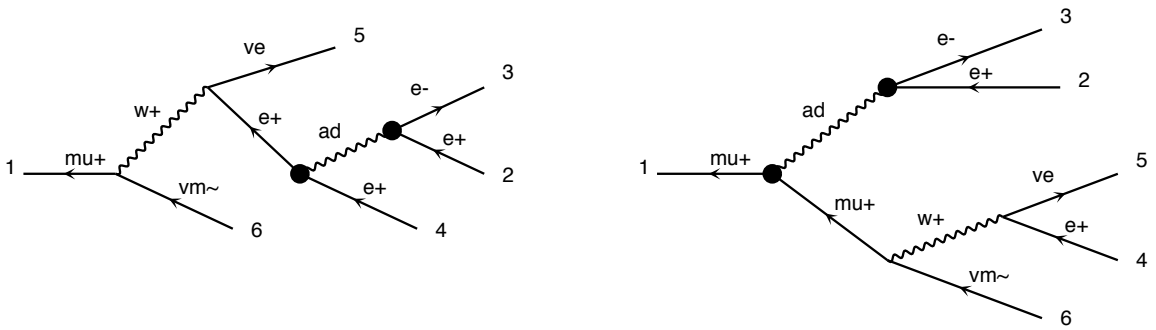

Figure B.3: Signal contribution to muon decay from the dark photon. The dark photon is taken to be on-shell where it decays to an e^+e^- pair.

B.2 e^+e^- Collisions at B-factories

Here we present all the diagrams generated by MadGraph in the calculations of e^+e^- collision cross sections.

B.2.1 Standard Model Background

We only show a portion of the diagrams in Fig. B.4 for the SM background process $e^+e^- \to \tau^+\tau^- e^+e^-$, as there are many diagrams.

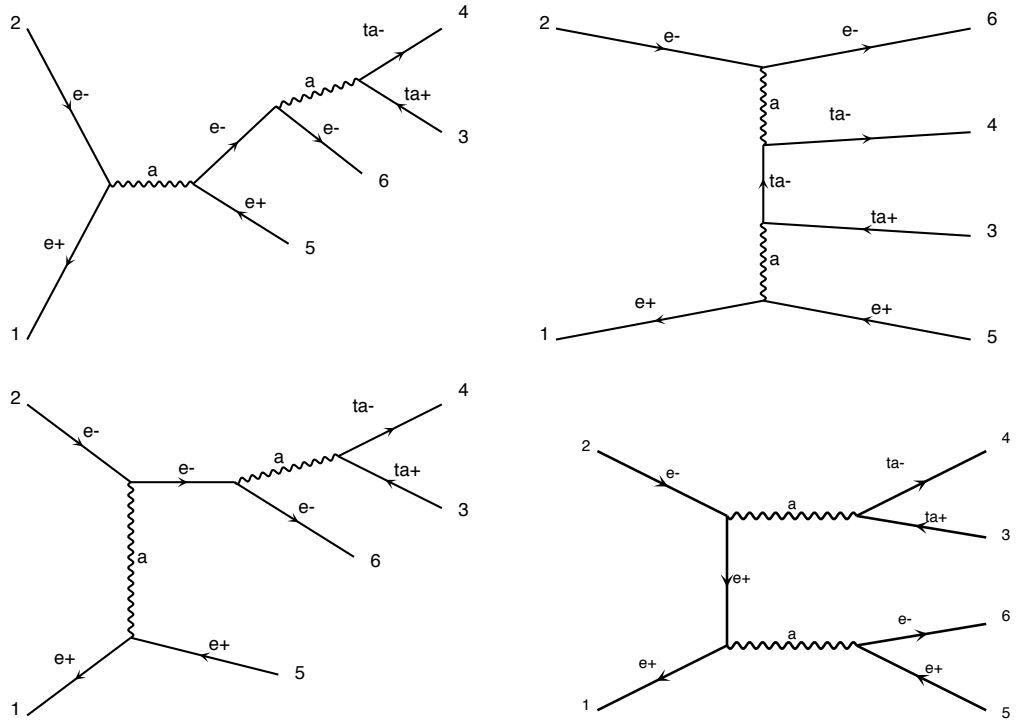

Figure B.4: A sample collection of the diagrams generated by MadGraph for the process $e^+e^- \to \tau^+\tau^- e^+e^-$. There are variants on these diagrams not included such as twists of these diagrams, replacements of the photon with a Z-boson, loops travelling in opposite directions, and also a final state with muons instead of electrons.

B.2.2 Scalar Signal

The diagrams shown in Fig. B.5 are used to compute the signal portion of the study.

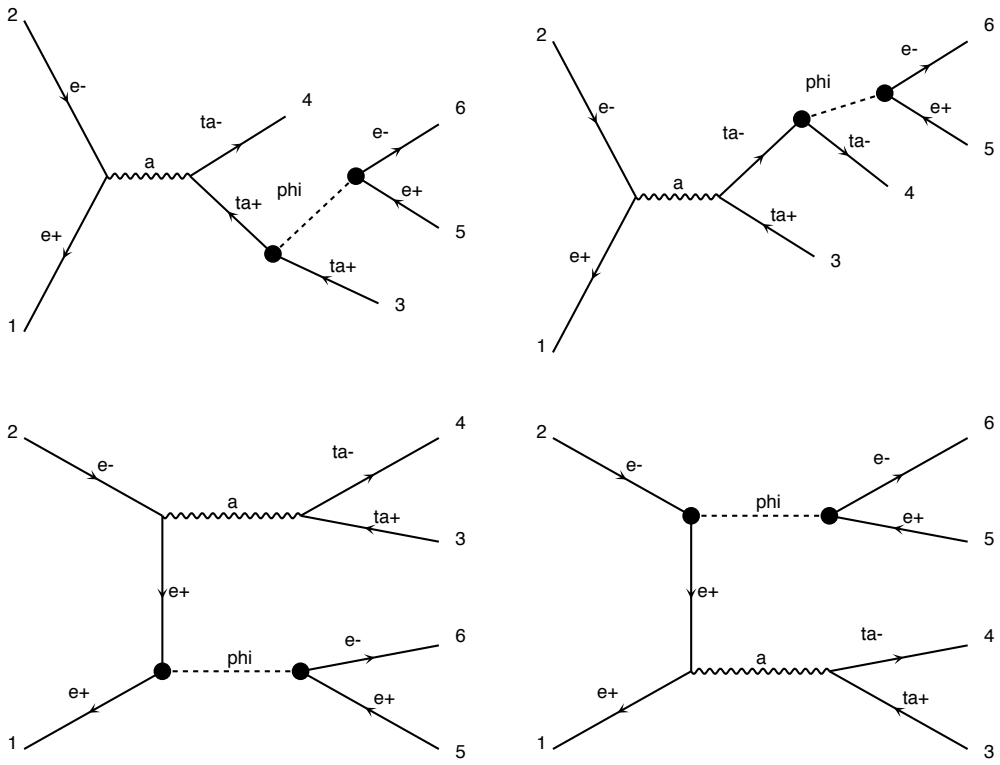

Figure B.5: e^+e^- annihilation to $\tau^+\tau^-e^+e^-$. We also generate the same diagrams but with a pair $\mu^+\mu^-$ instead in the final state. One can also replace a photon in each of the diagrams with a Z to reconstruct the full set of diagrams used. The scalar is taken to be on-shell where it decays to an e^+e^- pair.

Bibliography

[1] Raymond Davis, Jr., Don S. Harmer, and Kenneth C. Hoffman. Search for neutrinos from the sun. *Phys. Rev. Lett.*, 20:1205–1209, 1968.

[2] J. N. Abdurashitov et al. Measurement of the solar neutrino capture rate with gallium metal. *Phys. Rev.*, C60:055801, 1999.

[3] W. Hampel et al. GALLEX solar neutrino observations: Results for GALLEX IV. *Phys. Lett.*, B447:127–133, 1999.

[4] J. Boger et al. The Sudbury neutrino observatory. *Nucl. Instrum. Meth.*, A449:172–207, 2000.

[5] Y. Fukuda et al. Solar neutrino data covering solar cycle 22. *Phys. Rev. Lett.*, 77:1683–1686, 1996.

[6] S. Fukuda et al. Determination of solar neutrino oscillation parameters using 1496 days of Super-Kamiokande I data. *Phys. Lett.*, B539:179–187, 2002.

[7] V. N. Gribov and B. Pontecorvo. Neutrino astronomy and lepton charge. *Phys. Lett.*, B28:493, 1969.

[8] K. Hagiwara, A. D. Martin, D. Nomura, and T. Teubner. Improved predictions for g-2 of the muon and α(MZ2). *Physics Letters B*, 649:173–179, May 2007.

[9] R. Bayes et al. Experimental Constraints on Left-Right Symmetric Models from Muon Decay. *Phys. Rev. Lett.*, 106:041804, 2011.

[10] G. Czapek et al. Branching ratio for the rare pion decay into positron and neutrino. *Phys. Rev. Lett.*, 70:17–20, 1993.

[11] Mario Antonelli et al. Precision tests of the Standard Model with leptonic and semileptonic kaon decays. In *PHIPSI08, proceedings of the International Workshop on e+e- Collisions from phi to psi, Frascati (Rome) Italy, 7-10 April 2008*, 2008.

[12] G. Alexander et al. Measurement of the Z^0 line shape parameters and the electroweak couplings of charged leptons. *Z. Phys.*, C52:175–208, 1991.

[13] Carl E. Carlson. The Proton Radius Puzzle. *Prog. Part. Nucl. Phys.*, 82:59–77, 2015.

[14] Sergey Alekhin et al. A facility to Search for Hidden Particles at the CERN SPS: the SHiP physics case. 2015.

[15] Peter J. Mohr, Barry N. Taylor, and David B. Newell. CODATA Recommended Values of the Fundamental Physical Constants: 2010. *Rev. Mod. Phys.*, 84:1527–1605, 2012.

[16] Randolf Pohl et al. The size of the proton. *Nature*, 466:213–216, 2010.

[17] Aldo Antognini et al. Proton Structure from the Measurement of $2S - 2P$ Transition Frequencies of Muonic Hydrogen. *Science*, 339:417–420, 2013.

[18] Gerald A. Miller. Proton Polarizability Contribution: Muonic Hydrogen Lamb Shift and Elastic Scattering. *Phys. Lett.*, B718:1078–1082, 2013.

[19] Katherine Mesick. The MUSE Experiment: Studying the Proton Radius Puzzle with muon-proton Elastic Scattering. *PoS*, NUFACT2014:091, 2015.

[20] Ashot Gasparian. The PRad experiment and the proton radius puzzle. *EPJ Web Conf.*, 73:07006, 2014.

[21] Tatsumi Aoyama, Masashi Hayakawa, Toichiro Kinoshita, and Makiko Nio. Tenth-Order QED Contribution to the Electron g-2 and an Improved Value of the Fine Structure Constant. *Phys. Rev. Lett.*, 109:111807, 2012.

[22] Fred Jegerlehner and Andreas Nyffeler. The Muon g-2. *Phys. Rept.*, 477:1–110, 2009.

[23] Kaoru Hagiwara, A. D. Martin, Daisuke Nomura, and T. Teubner. Improved predictions for g-2 of the muon and alpha(QED) (M**2(Z)). *Phys. Lett.*, B649:173–179, 2007.

[24] Andrzej Czarnecki and William J. Marciano. The Muon anomalous magnetic moment: A Harbinger for 'new physics'. *Phys. Rev.*, D64:013014, 2001.

[25] Graziano Venanzoni. The New Muon g-2 experiment at Fermilab. In *37th International Conference on High Energy Physics (ICHEP 2014) Valencia, Spain, July 2-9, 2014*, 2014.

[26] Andreas Juttner and Michele Della Morte. New ideas for g-2 on the lattice. *PoS*, LAT2009:143, 2009.

[27] Dru B. Renner, Xu Feng, Karl Jansen, and Marcus Petschlies. Leading order hadronic contribution to g-2 from twisted mass QCD. *PoS*, LATTICE2010:155, 2010.

[28] Rehan Malak, Zoltan Fodor, Christian Hoelbling, Laurent Lellouch, Alfonso Sastre, and Kalman Szabo. Finite-volume corrections to the leading-order hadronic contribution to $g_\mu - 2$. *PoS*, LATTICE2014:161, 2015.

[29] J. D. Bjorken, S. Ecklund, W. R. Nelson, A. Abashian, C. Church, B. Lu, L. W. Mo, T. A. Nunamaker, and P. Rassmann. Search for Neutral Metastable Penetrating Particles Produced in the SLAC Beam Dump. *Phys. Rev.*, D38:3375, 1988.

[30] Brian Batell, Nicholas Lange, David McKeen, Maxim Pospelov, and Adam Ritz. The Leptonic Higgs Portal. work in progress.

[31] James D. Bjorken, Rouven Essig, Philip Schuster, and Natalia Toro. New Fixed-Target Experiments to Search for Dark Gauge Forces. *Phys. Rev.*, D80:075018, 2009.

[32] A. Blondel et al. Research Proposal for an Experiment to Search for the Decay $\mu \to eee$. 2013.

[33] M. L. Brooks et al. New limit for the family number nonconserving decay $\mu^+ \to e^+\gamma$. *Phys. Rev. Lett.*, 83:1521–1524, 1999.

[34] J. Adam et al. New limit on the lepton-flavour violating decay $\mu^+ \to e^+\gamma$. *Phys. Rev. Lett.*, 107:171801, 2011.

[35] U. Bellgardt et al. Search for the Decay $\mu^+ \to e^+e^+e^-$. *Nucl. Phys.*, B299:1, 1988.

[36] Wilhelm H. Bertl et al. A Search for muon to electron conversion in muonic gold. *Eur. Phys. J.*, C47:337–346, 2006.

[37] K. A. Olive et al. Review of Particle Physics. *Chin. Phys.*, C38:090001, 2014.

[38] R. Batley et al. Precision measurement of charged kaon decay parameters with an extended NA48 setup. (Addendum 3 to Proposal P253/CERN/SPSC). 1999.

[39] Silvia Martellotti. The NA62 Experiment at CERN. In *12th Conference on the Intersections of Particle and Nuclear Physics (CIPANP 2015) Vail, Colorado, USA, May 19-24, 2015*, 2015.

[40] Evgueni Goudzovski. Search for the dark photon in π^0 decays by the NA48/2 experiment at CERN. *EPJ Web Conf.*, 96:01017, 2015.

[41] David M. Straub. New physics correlations in rare decays. In *CKM unitarity triangle. Proceedings, 6th International Workshop, CKM 2010, Warwick, UK, September 6-10, 2010*, 2010.

[42] D. Boutigny et al. BaBar technical design report. 1995.

[43] M. T. Cheng et al. A Study of CP violation in B meson decays: Technical design report. 1995.

[44] T. Abe et al. Belle II Technical Design Report. 2010.

[45] A. G. Akeroyd et al. Physics at super B factory. 2004.

[46] Bob Holdom. Two U(1)'s and Epsilon Charge Shifts. *Phys. Lett.*, B166:196, 1986.

[47] Maxim Pospelov. Secluded U(1) below the weak scale. *Phys. Rev.*, D80:095002, 2009.

[48] J. R. Batley et al. Search for the dark photon in π^0 decays. *Phys. Lett.*, B746:178–185, 2015.

[49] Bertrand Echenard, Rouven Essig, and Yi-Ming Zhong. Projections for Dark Photon Searches at Mu3e. *JHEP*, 01:113, 2015.

[50] Abner Soffer. Searches for Light Scalars, Pseudoscalars, and Gauge Bosons. In *13th Conference on Flavor Physics and CP Violation (FPCP 2015) Nagoya, Japan, May 25-29, 2015*, 2015.

[51] Abdelhak Djouadi. The Anatomy of electro-weak symmetry breaking. I: The Higgs boson in the standard model. *Phys. Rept.*, 457:1–216, 2008.

[52] Jacques P. Leveille. The Second Order Weak Correction to (G-2) of the Muon in Arbitrary Gauge Models. *Nucl. Phys.*, B137:63, 1978.

[53] David McKeen. Contributions to the Muon's Anomalous Magnetic Moment from a Hidden Sector. *Annals Phys.*, 326:1501–1514, 2011.

[54] David Tucker-Smith and Itay Yavin. Muonic hydrogen and MeV forces. *Phys. Rev.*, D83:101702, 2011.

[55] Adam Alloul, Neil D. Christensen, Céline Degrande, Claude Duhr, and Benjamin Fuks. FeynRules 2.0 - A complete toolbox for tree-level phenomenology. *Comput. Phys. Commun.*, 185:2250–2300, 2014.

[56] R. Mertig, M. Bohm, and Ansgar Denner. FEYN CALC: Computer algebraic calculation of Feynman amplitudes. *Comput. Phys. Commun.*, 64:345–359, 1991.

[57] Johan Alwall, Michel Herquet, Fabio Maltoni, Olivier Mattelaer, and Tim Stelzer. MadGraph 5 : Going Beyond. *JHEP*, 06:128, 2011.

[58] J. Alwall, R. Frederix, S. Frixione, V. Hirschi, F. Maltoni, O. Mattelaer, H. S. Shao, T. Stelzer, P. Torrielli, and M. Zaro. The automated computation of tree-level and next-to-leading order differential cross sections, and their matching to parton shower simulations. *JHEP*, 07:079, 2014.

[59] Celine Degrande, Claude Duhr, Benjamin Fuks, David Grellscheid, Olivier Mattelaer, and Thomas Reiter. UFO - The Universal FeynRules Output. *Comput. Phys. Commun.*, 183:1201–1214, 2012.

[60] Torbjorn Sjostrand, Stephen Mrenna, and Peter Z. Skands. A Brief Introduction to PYTHIA 8.1. *Comput. Phys. Commun.*, 178:852–867, 2008.

[61] Michele Selvaggi. DELPHES 3: A modular framework for fast-simulation of generic collider experiments. *J. Phys. Conf. Ser.*, 523:012033, 2014.

[62] S. Agostinelli et al. GEANT4: A Simulation toolkit. *Nucl. Instrum. Meth.*, A506:250–303, 2003.

[63] M. Schulz, D. Fischer, T. Ferger, R. Moshammer, and J. Ullrich. Four-particle Dalitz plots to visualize atomic break-up processes. *Journal of Physics B Atomic Molecular Physics*, 40:3091–3099, August 2007.

[64] H. Murayama, I. Watanabe, and Kaoru Hagiwara. HELAS: HELicity amplitude subroutines for Feynman diagram evaluations. 1992.

[65] Priscila de Aquino, William Link, Fabio Maltoni, Olivier Mattelaer, and Tim Stelzer. ALOHA: Automatic Libraries Of Helicity Amplitudes for Feynman Diagram Computations. *Comput. Phys. Commun.*, 183:2254–2263, 2012.

[66] Johan Alwall et al. A Standard format for Les Houches event files. *Comput. Phys. Commun.*, 176:300–304, 2007.

[67] Flip Tanedo. Monte carlo with madgraph, personal notes and how-to guide. `http://www.physics.uci.edu/~tanedo/files/notes/ColliderMadgraph.pdf`, August 2011. [Online; accessed 11-December-2015].

[68] K. O. Mikaelian and J. Smith. Radiative corrections to the decay pi0 $\rightarrow$ gamma e+ e-. *Phys. Rev.*, D5:1763–1773, 1972.

[69] J. P. Lees et al. Search for a Dark Photon in e^+e^- Collisions at BaBar. *Phys. Rev. Lett.*, 113(20):201801, 2014.

[70] R. J. Abrams et al. Mu2e Conceptual Design Report. 2012.

[71] Y. G. Cui et al. Conceptual design report for experimental search for lepton flavor violating mu- - e- conversion at sensitivity of 10**(-16) with a slow-extracted bunched proton beam (COMET). 2009.